MODELLING A JANUS PARTICLE ACTIVATED BY AN OPTICAL POTENTIAL

A THESIS SUBMITTED TO

THE GRADUATE SCHOOL OF ENGINEERING AND SCIENCE

OF BILKENT UNIVERSITY

IN PARTIAL FULFILLMENT OF THE REQUIREMENTS FOR

THE DEGREE OF

MASTER OF SCIENCE

IN

MECHANICAL ENGINEERING

By

Umar Rauf

September 2023

Modelling a Janus particle activated by an optical potential
By Umar Rauf
September 2023

We certify that we have read this thesis and that in our opinion it is fully adequate, in scope and in quality, as a thesis for the degree of Master of Science.

Luca Biancofiore(Advisor)

Emine Yegan Erdem

Mirko Indro Gallo

Approved for the Graduate School of Engineering and Science:

Orhan Arıkan
Director of the Graduate School

ABSTRACT

MODELLING A JANUS PARTICLE ACTIVATED BY AN OPTICAL POTENTIAL

Umar Rauf
M.S. in Mechanical Engineering
Advisor: Luca Biancofiore
September 2023

The flow around a Janus particle under an optical potential is investigated. The thermal effects are majorly overlooked while studying the Janus particle although fluid heating caused by optical potential might negligible but the fluid heating caused due to Janus particle acting as a heating source is not negligible. The stream function approach is used to model the behavior of an activated Janus particle. The explicit finite difference method (FDM) is used to numerically obtain the solution. BIL-FLOW, an in-house FDM code is developed and validated for flow around a Janus particle under an optical potential. Additionally, The BIL-OP, an in-house optical module based on geometric ray approximation is developed and validated. BIL-OP utilizes linear algebra to calculate three dimensional (3D) optical force.

Keywords: Janus Particle, Computational Fluid Dynamics, Geometrical Optics.

ÖZET

OPTIK POTENSIYEL TARAFINDAN ETKINLEşTIRILEN JANUS PARÇACIğI MODELLENMESI

Umar Rauf
Makine Mühendisliği, Yüksek Lisans
Tez Danışmanı: Luca Biancofiore
Eylül 2023

Janus parçacığı etrafındaki akış optik potansiyel altında araştırıldı. Janus parçacığını incelerken termal etkiler büyük ölçüde göz ardı edilir. Optik potansiyelin neden olduğu sıvı ısınması ihmal edilebilir düzeyde olmayabilir ancak sıvı ısınması Janus parçacığının bir ısıtma kaynağı olarak hareket etmesinden kaynaklanan nedenler göz ardı edilemez. Akış fonksiyonu yaklaşımı, etkinleştirilmiş bir Janus parçacığının davranışını modellemek için kullanılır. Çözümü sayısal olarak elde etmek için açık sonlu farklar yöntemi (FDM) kullanılır. BIL-FLOW, şirket içi bir FDM kodu, optik potansiyel altında Janus parçacığı etrafındaki akış için geliştirildi ve doğrulandı. BIL-OP, geometrik ışın yaklaşımına dayanan şirket içi bir optik modülü, geliştirildi ve doğrulandı. BIL-OP, üç boyutlu (3D) optik kuvveti hesaplamak için doğrusal cebirden yararlanır.

Anahtar sözcükler: Janus Parçacığı, Hesaplamalı Akışkanlar Dinamiği, Geometrik Optik.

Acknowledgement

I would like to express my sincere thanks and gratitude to Dr. Luca Biancofiore for his constant support and guidance during the course of this study.

The scholarship and support awarded from TUBITAK is greatly appreciated and acknowledged under project No.119N461.

Thanks are also extended to all of my teachers, staff and colleagues at Bilkent University and members of Fluidframe-Lab especially Dr. Emine Yegan Erdem, Dr Seymur Jahangirov , (soon to be) Dr. Humayun Ahmed, Dr. Agnese Callegari (External), Dr. Mirko Indro Gallo (External) and Miss Ela Baycan for their help, willing support, motivation and useful discussions I had with them.

Thanks are also extended to all my friends especially Talha Arshad, Abdullah Habboush, S.M. Hassan Askari Zaidi, Tokzhan Karatai, Sana Basharat, Talha Ejaz, M. Hilal Khan, Asfandyar Khan, Muzaffer Rafique, Maryam Jamil, M. Zain Siddiqui, Bilal Ali, Hamza Fiaz, Moaqir Ahmed Mian and Muneebullah Nawaz for all their guidance, support, motivation, meaningful and useful discussion I had with them and for their criticisms.

Finally, I must express my profound appreciation to members of my family for their encouragement, patience and generous help in many ways.

To Mom and Dad (In Heaven)

Contents

List of Figures

List of Tables

Chapter 1

Introduction

The problem at hand ,flow past a activated Janus particle, is multidisciplinary spanning the domains of fluid mechanics, physics, optics and particle dynamics. This thesis majorly focuses and contributes to the field of fluid mechanics and optics. Particularly. we focused on the thermal effect around a activated Janus particle and utilized Boussinesq-approximation to investigate the effect of optical potential on a janus particle.

External flow over bodies has been a fundamental problem of fluid mechanics and an area of interest for physicists,mathematicians and engineers alike for a long time. The Navier-Stokes equation are used to solve problems ranging from blood flow through the arteries in heart to weather,rivers and space patterns. [1–3].The flow around a sphere was first investigated by Stokes almost two centuries ago. he calculated the solution in condition that the Reynolds number is very small or flow in which the viscous force are highly dominating the inertial forces. [1]. Whitehead [4] solved the equation for case in which the Reynolds number is not very small. He obtained an higher order expansion in terms of Reynolds numbers. The procedure he developed was iterative which calculated the inertial terms in equation of motion. The procedure involved expansion of the flow in power of Reynolds number. He showed that the second expansion of velocity remains finite at infinity and does not satisfy the boundary condition at infinity in other words, Higher approximation of velocity diverges at infinity [5]. The expansion of flow in powers of Reynolds number breakdown's and is widely known as the whitehead Paradox. The Whitehead Paradox was later resolved by Oseen. He linearized the inertial term far from the sphere. He showed that the approximation of velocity and its derivatives is a linear problem and it can be solved analytically [6]. The same problem was also investigated by Kaplun and Lagerstrom [7] who used method of matched asymptotic expansions, which was later utilized by Proudman and Pearson to obtain higher order approximate solution of flow past a sphere and cylinder. They noted that it is possible to obtain finite number of terms which provides solution of required accuracy but this does not apply to successive term in higher order uniform approximation [5].

Many problems in fluid mechanics were solved by using the method of matched asymptotic expansions.Van Dyke also utilized this method to obtain solution of viscous flow at low Reynolds numbers [8]. He matched the expansion of Stokes's with Oseen's to solve the Whitehead paradox. The same method was also utilized by Kohr to solve in-compressible low Reynolds flow around a cylinder [9]. Umemura used this to solve flow past two cylinders under low Reynolds flow [10]. Datta and Singhal extended this by solving fluid flow past a sphere source at it's centre. He obtain the solution of the Navier-Stokes Equations with matched asymptotic expansions method by applying the stream function formulation with vorticity. He established the Stokes's expansion as inner expansion and Oseen's expansion as outer expansion. He used inner and outer expansion to obtain the undetermined coefficients in both expansions and was able to obtain higher order expansions [11].

The finite difference method (FDM) is a numerical technique which is used to obtain solutions of partial differential equations (PDEs) by approximating the derivatives in PDEs. The method is easier to implement for simpler geometries (sphere,cylinder etc) and domains (rectangular,cylindrical,spherical etc) but becomes complicated for complex geometries. A number of authors used FDM to obtain solutions of in-compressible and compressible flow past a sphere and cylinder. [12] Chorin applied FDM to solve Navier-Stokes equations for incompressible fluid. He realized the capability of the use of FDM for problems having two and three dimensional space. The numerical solution of the steady viscous flow past a stationary deformable bubble was presented by Christov and Volkov [13]. They applied a coordinate transformation such that the unknown region can be mapped to a known region and infinity was approximated by a large value. Hence, the boundary condition was satisfied. They used second-order finite difference approximation and their solutions were in good agreement with theoretical and experimental results. Fornberg obtained the numerical solution of the steady incompressible flow past a sphere. The Steady-State (SS) Navier-Stokes equations were used to describe the equations of motion. The SS Navier-Stokes equations were rewritten in terms of Vorticity and stream function in cylindrical coordinate system and solved using central second-order finite difference scheme [14]. The wakes took the form of Hill's spherical vortex. A similar work was carried out by Zhang to solve driven cavity. He solved SS Navier-Stokes equations in primitive variables using FDM, The non-linear terms were discretized by combination of second-order forward and backward finite difference schemes while the linear terms were discretized by the second-order central difference scheme. The systems of equations obtained were then solved by the multi grid method. The results were agreement with vorticity-stream function results [15]. Juncu also worked on Steady viscous flow past a sphere. The unique aspect of his work was that he used the non-dimensional vorticity-stream function formulation in spherical coordinates and he studied Reynolds up-to 500. He utilized second-order central finite difference scheme as it predicts the flow accurately and he observed that the convergence decreased with decrease in Reynolds. The results obtained were comparable to those present in literature [16]. Lai also used vorticity-stream function formulation and developed a fourth-order finite difference scheme to solve incompressible Navier-Stokes equations in a disk, their results agreed with studies carried out previously [17]. Li and Wang similarly applied vorticity-stream function formulation and used fast finite difference method to solve incompressible Navier-Stokes equations in irregular domains on a Cartesian grid as aforementioned grid is suitable for solving complex geometries. The results showed that the numerical solutions obtained were second-order accurate [18].

The aim of this thesis is to revisit the problem of flow past a sphere and derive the dimensionless Navier-Stokes equations using the vorticity-stream function with a coordinate transformation and validate the model with existing literature [19]. The Boussinesq approximation (the density difference is ignored except where they come in terms multiplied by gravity) named after Joseph Valentin Boussinesq and used for buoyancy driven flows will then be similarly derived in vorticity-stream function formulation. Additionally, the dimensionless energy equation will be solved for the fluid and solid sphere separately, The major difference being that the energy equation in solid sphere will have the optical potential acting as the source term, which for this work will be approximated as Gaussian profile to replicate a Gaussian beam. The final step will be to treat the sphere as a Janus particle and The source term will be acting only on one half of the sphere. The non-dimensionalized equations will then be solved using central second-order finite difference approximation and The optics module will also be developed and validated with existing Literature which will calculate the force and torque on a spherical Janus particle.

This thesis is organized as follows. Chapter 2 Computational Modelling of fluid in presence of Janus Particle and analyses the effect of different parameters on fluid behavior around Janus sphere. Chapter 3 Geometrical Ray Approximation for optical tweezers under different optical potential explores the optical effect upon the model. In Chapter 4, we present a novel memory architecture that can make use of stored data about the transients of previously experienced anomalies to aid in obtaining a resilient adaptive control system. Finally, a conclusion is provided in Chapter 5. Throughout the thesis, for all the modules and numerical simulations carried out the results are summarized and concluded.

Chapter 2

Modelling Thermal Distribution around an Activated Janus Particle

2.1 Introduction

The Stokes flow, a key presumption for the behavior of the fluid regime, is a fundamental framework used in this study. According to the Stokes flow regime, inertial fluid forces are small in comparison to viscous forces. This presumption is consistent with low Reynolds number conditions, such as those that frequently occur in microfluidics or when working with extremely viscous fluids. The study tries to simplify the governing equations and focus on the dominating viscous forces at work by using the Stokes flow assumption.

By simultaneously solving momentum and energy equations for the particle and the surrounding fluid, the current study addresses the complex interactions between a solid object and a fluid medium. This strategy seeks to understand the complex dynamics at the solid-fluid interface, encompassing the interactions between forces and energy exchange events.

The Boussinesq approximations have also been used to simplify the mathematical study of thermal effects in the fluid medium. The ability to represent density fluctuations as linear functions of temperature deviations is made possible by these approximations, which are useful in situations where temperature differences in the fluid are modest compared to its average temperature. The original momentum and energy equations can be simplified in this way, leading to a more manageable mathematical framework that more accurately captures the nature of physical reality.

The integration of the energy equation with the derivation founded on the Stokes flow premise is an important extension of this conceptual framework. In order to account for thermal impacts, the Stokes flow's basic presumptions must be expanded. The study aims to describe the complex interplay between the solid and fluid entities while accounting for temperature fluctuations by integrating the energy equation, which captures the transmission of thermal energy, with the Stokes flow basis. This coupling broadens the analytical focus and offers a more thorough insight of the behavior of the system.

2.1.1 Notations

We denote the $(\cdot)$ to represent the dot product and use $(\times)$ to denote the cross product. $\sum$ represents the summation. The 'Re' and 'Gr' represents the Reynolds and Grashoff numbers respectively. ∇, E and $e^{2Z}E^2$ represents the operators. The bold characters represents the vector quantities. The subscript usually represents the components of vectors.

2.2 Problem Statement

To model the behavior of an activated Janus sphere in two configurations while applying the Boussinesq approximation. The continuity, momentum and energy equations were solved for the fluid around a Janus sphere while the energy equation in the solid sphere with a Gaussian beam acting as a source term is coupled with the fluid's energy equation and this coupling broadens the stokes flow and offer's a more deep insight while considering the effect of Grashoff system.

2.3 Governing Equations

The governing equations for a stokes flow consists of the conservation of mass

$$\nabla \cdot \mathbf{u} = 0, \tag{2.1}$$

The momentum/Boussinesq equation (conservation of momentum) of motion reads (Steady State, also using continuity),

$$(\mathbf{u}.\nabla)\mathbf{u} = \frac{(-\nabla p)}{\rho_0} + \nu\nabla^2\mathbf{u} + \frac{\rho\boldsymbol{g}}{\rho_0}, \tag{2.2}$$

In this equation, density variations are assumed to have a fixed part and another part that has a linear dependence on temperature given as $\rho = \rho_0 - \rho_0\alpha(T - T_0)$, where α is the coefficient of thermal expansion. The Boussinesq approximation states that the density variation is only important in the buoyancy term. The final equation becomes

$$(\nabla.\mathbf{u})\mathbf{u} = -\frac{1}{\rho_0}\nabla(p - \rho_0\boldsymbol{g} \cdot \boldsymbol{z}) + \nu\nabla^2\mathbf{u} - \boldsymbol{g}\alpha(T - T_0), \tag{2.3}$$

where $\mathbf{u}$ is the velocity field, $\boldsymbol{g}$ is the gravity,ρ is the density and ν is the kinematic viscosity.

The temperature profile for the Janus particle is derived using the Fourier's law (Steady State) which is derived by Thomas Bickel [20], which is, Here we merely quote the temperature profile in the liquid phase ($r > a$):

$$T(r, \theta) = T_0 + \frac{\Delta T}{\pi}\sum_{n=0}^{+\infty} t_n P_n(c)(\frac{a}{r})^{n+1} \tag{2.4}$$

with $c = \cos\theta$ and Legendre polynomial P_n. The coefficients t_n are given by

$$t_{2k} = -t_{2k+1} = \frac{(-1)^k}{2k+1}$$

where t_0=1+$\frac{\pi}{2}$,Identifying the power P absorbed by the metal cap with the total outward heat flow, one readily establishes the relation with the excess temperature: P=(2π+4)kaΔT.
The energy equation solved by [20] is,

$$k\nabla^2 T = q(r) \tag{2.5}$$

where q is the power absorbed by the metal cap side of the sphere, and k is the thermal conductivity of the particle and surrounding (taken as same).The cap conductivity k_c is usually much higher than k; if their ratio is larger than the ratio of particle radius and cap thickness, $k_c/k > a/d$, the cap forms an isotherm.

The energy equation for the particle as well as the fluid will be solved separately,and the solid and fluid will communicate with each other through flux boundary condition. The energy equation for both medium are explained below:
The energy equation for the particle is,

$$k_p\nabla^2 T_p + q(r) = 0 \tag{2.6}$$

The energy equation for the fluid is,

$$k_f\nabla^2 T_f = (\mathbf{u}.\nabla)T_f \tag{2.7}$$

where k_p and k_f are the thermal conductivity of the particle and the surrounding fluid respectively. Now we use momentum equation to obtain the solution of Boussinesq approximation (through Stream Function).

Referring to the spherical coordinates system (r,θ,ϕ) as in figure. 2.1. Let the ambient velocity be upward and along the polar (z) axis: (u,v,w)=(0,0,W) while the gravity $\mathbf{g}$ is directed downwards. Axial symmetry demands

$$\frac{\partial}{\partial\phi} = 0, and\ \boldsymbol{u} = (u_r(r,\theta), u_\theta(r,\theta), 0)$$

Continuity equation becomes,

$$\frac{1}{r^2}\frac{\partial}{\partial r}(r^2 u_r) + \frac{1}{r}\frac{\partial}{\partial\theta}(u_\theta \sin\theta) = 0 \tag{2.8}$$

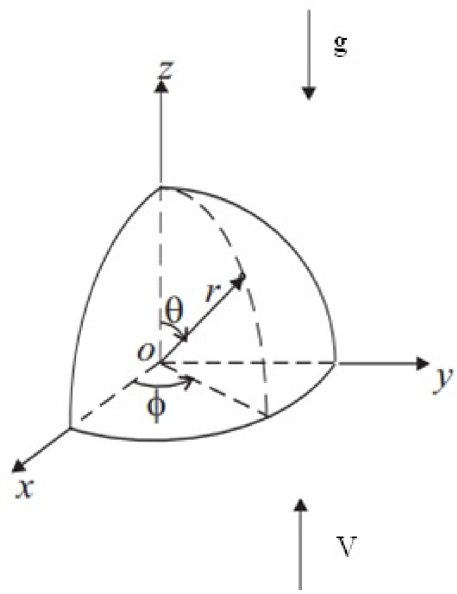

Figure 2.1: Spherical Coordinates.

As in the case of rectangular coordinates, we define the stream function ψ to satisfy the continuity equation identically

$$u_r = \frac{1}{r^2 \sin\theta}\frac{\partial\psi}{\partial\theta},\ u_\theta = -\frac{1}{r\sin\theta}\frac{\partial\psi}{\partial r} \tag{2.9}$$

At infinity, the uniform velocity W along z axis can be decomposed into radial and polar components

$$u_r = W\cos\theta = \frac{1}{r^2 \sin\theta}\frac{\partial\psi}{\partial\theta},\ u_\theta = -W\sin\theta = -\frac{1}{r\sin\theta}\frac{\partial\psi}{\partial r},\ r\sim\infty \tag{2.10}$$

The corresponding stream function at infinity follows by integration

$$\psi = \frac{W}{2}r^2\sin^2\theta,\ r\sim\infty \tag{2.11}$$

Using the vector identity,

$$\nabla\times(\nabla\times\boldsymbol{u}) = \nabla(\nabla\cdot\boldsymbol{u}) - \nabla^2\boldsymbol{u},$$

$$(\mathbf{u}.\nabla)\mathbf{u} = \nabla(\frac{1}{2}\mathbf{u}^2) - \mathbf{u}\times(\nabla\times\mathbf{u})$$

this becomes utilizing continuity

$$\nabla^2\boldsymbol{u} = -\nabla\times(\nabla\times\boldsymbol{u}) = -\nabla\times\boldsymbol{\zeta}$$

$$\nabla^2 \boldsymbol{u} = -\nabla \times \boldsymbol{\zeta}$$

Taking the curl of momentum equation (2.3) and using the identity derived, we obtain

$$\nabla \times (\mathbf{u}.\nabla)\mathbf{u} = \nabla \times -\frac{1}{\rho_0}\nabla(p - \rho_0 \boldsymbol{g} \cdot \boldsymbol{z}) + \nabla \times \nu\nabla^2\mathbf{u} - \nabla \times \boldsymbol{g}\alpha(T - T_0)$$

The equation simplifies to,

$$\nabla \times (\mathbf{u}.\nabla)\mathbf{u} = \nabla \times \nu\nabla^2\mathbf{u} - \nabla \times \boldsymbol{g}\alpha(T - T_0)$$

$$\nabla \times (\mathbf{u}.\nabla)\mathbf{u} + \nabla \times \boldsymbol{g}\alpha(T - T_0) = \nabla \times \nu\nabla^2\mathbf{u}$$

where α, ν are constants and ζ is vorticity, which is expressed as ζ=$\nabla \times \boldsymbol{u}$. For now consider the right side of the equation only

$$\nabla^2 \boldsymbol{u} = -\nabla \times \boldsymbol{\zeta}$$

$$R.H.S: \quad -\nu\nabla \times \nabla \times \boldsymbol{\zeta}, \tag{2.12}$$

$$-\nu\nabla \times \nabla \times \nabla \times \boldsymbol{u},$$

from straight forward algebra $\boldsymbol{u}$ can be obtained (basic Stokes-flow derivation)

$$\boldsymbol{u} = \nabla \times (\frac{\psi \boldsymbol{e_\phi}}{r\sin\theta}),$$

Substituting in equation 2.12 we obtain

$$-\nu\nabla \times \nabla \times \nabla \times \nabla \times (\frac{\psi \boldsymbol{e_\phi}}{r\sin\theta}) \tag{2.13}$$

The left side of the equation is

$$L.H.S: \nabla \times (\mathbf{u}.\nabla)\mathbf{u} + \alpha\nabla \times (T - T_0)\boldsymbol{g}, \tag{2.14}$$

now using the identity

$$\nabla \times \Psi\boldsymbol{A} = \Psi\nabla \times \boldsymbol{A} + (\nabla\Psi) \times \boldsymbol{A}$$

Where A is vector and Ψ is a scalar, equation 2.14 can be simplified as

$$\alpha[(T - T_0)\nabla \times \boldsymbol{g} + (\nabla(T - T_0) \times \boldsymbol{g})]$$

where $\nabla \times \boldsymbol{g}$ =0 (curl of gradient is zero), also using the identity

$$(\mathbf{u}.\nabla)\mathbf{u} = \nabla(\frac{1}{2}\mathbf{u}^2) - \mathbf{u} \times (\nabla \times \mathbf{u})$$

as ζ=$\nabla \times \boldsymbol{u}$.
Hence the L.H.S simplifies to

$$-\nabla \times (\mathbf{u} \times \zeta) + \alpha(\nabla(T - T_0) \times \boldsymbol{g} \tag{2.15}$$

expanding the cross product in spherical coordinates

$$\frac{(\alpha)}{r^2 \sin\theta} \begin{vmatrix} \boldsymbol{e_r} & r\boldsymbol{e_\theta} & r\sin\theta \boldsymbol{e_\phi} \\ \frac{\partial T}{\partial r} & \frac{\partial T}{\partial \theta} & 0 \\ -g\cos\theta & rg\sin\theta & 0 \end{vmatrix}$$

which can simplify to

$$\frac{(\alpha)}{r^2 \sin\theta}[r\sin\theta(\frac{\partial T}{\partial r} rg\sin\theta + \frac{\partial T}{\partial \theta} g\cos\theta)]\boldsymbol{e_\phi}$$

further simplification yields

$$-\nabla \times (\mathbf{u} \times \zeta) + \frac{(\alpha)}{r}(\frac{\partial T}{\partial r} rg\sin\theta + \frac{\partial T}{\partial \theta} g\cos\theta)\boldsymbol{e_\phi} \tag{2.16}$$

Hence the whole equation becomes

$$\begin{aligned} -\nu\nabla \times \nabla \times \nabla \times \nabla \times (\frac{\psi \boldsymbol{e_\phi}}{r\sin\theta}) &= -\nabla \times (\mathbf{u} \times \zeta)\boldsymbol{e_\phi} \\ &+ \frac{(\alpha)}{r}(\frac{\partial T}{\partial r} rg\sin\theta + \frac{\partial T}{\partial \theta} g\cos\theta)\boldsymbol{e_\phi} \end{aligned} \tag{2.17}$$

after equating for $\boldsymbol{e_\phi}$ it becomes a scalar equation for ψ, it is written as:

$$-\nabla\times(\mathbf{u}\times\zeta)+\frac{(\alpha)}{r}(\frac{\partial T}{\partial r} rg\sin\theta+\frac{\partial T}{\partial \theta} g\cos\theta) = -\nu\nabla\times\nabla\times\nabla\times\nabla\times(\frac{\psi}{r\sin\theta}) \tag{2.18}$$

After expanding the equation, the final equation is

$$\begin{aligned} &\left[\frac{\partial \psi}{\partial r} \cdot \frac{\partial}{\partial \theta}\left(\frac{E^2\psi}{r^2\sin^2\theta}\right) - \frac{\partial \psi}{\partial \theta} \cdot \frac{\partial}{\partial r}\left(\frac{E^2\psi}{r^2\sin^2\theta}\right)\right]\sin\theta - \\ &\alpha g[\frac{\partial T}{\partial r} r\sin\theta + \frac{\partial T}{\partial \theta}\cos\theta]\sin\theta = \nu E^4\psi \end{aligned} \tag{2.19}$$

where

$$E^2 = \frac{\partial^2}{\partial r^2} + \frac{\sin\theta}{r^2}\frac{\partial}{\partial \theta}(\frac{1}{\sin\theta}\frac{\partial}{\partial \theta}) \tag{2.20}$$

The final equation (2.19) may be split into two simultaneous second order equations by introducing vorticity ζ as

$$E^2\psi = \zeta r \sin\theta \tag{2.21}$$

$$\begin{gathered}\left[\frac{\partial\psi}{\partial r}\cdot\frac{\partial}{\partial\theta}\left(\frac{\zeta}{r\sin\theta}\right) - \frac{\partial\psi}{\partial\theta}\cdot\frac{\partial}{\partial r}\left(\frac{\zeta}{r\sin\theta}\right)\right]\sin\theta - \\ \alpha g[\frac{\partial T}{\partial r} r\sin\theta + \frac{\partial T}{\partial\theta}\cos\theta]\sin\theta = \nu E^2(\zeta r\sin\theta)\end{gathered} \tag{2.22}$$

2.3.1 Non-Dimensionalized Equations

The non-dimensional parameters are:

$$r^* = \frac{r}{A}$$

$$\nabla^* = A\nabla$$

$$U^* = \frac{u}{U}$$

$$P^* = \frac{PA}{\mu U}$$

$$T^* = \frac{T - T_0}{\Delta T}$$

$$Q = \frac{qA^2}{k\Delta T}$$

where Re: Reynolds number=$\frac{2UA}{\nu}$, Gr: Grashoff number=$\frac{g\alpha\Delta T A^3}{\nu^2}$ and Pr: Prandtl number=$\frac{C_p\mu}{k}$, using the equations 2.3 and obtaining 2.19, and subsituting ζ to reach 2.21 2.22 we obtain the dimensionless equations for momentum which is:

$$\begin{gathered}E^2\psi = \zeta r\sin\theta \\ \frac{Re}{2}\left[\frac{\partial\psi}{\partial r}\cdot\frac{\partial}{\partial\theta}\left(\frac{\zeta}{r\sin\theta}\right) - \frac{\partial\psi}{\partial\theta}\cdot\frac{\partial}{\partial r}\left(\frac{\zeta}{r\sin\theta}\right)\right]\sin\theta - \\ 2Gr[\frac{\partial T^*}{\partial r} r\sin\theta + \frac{\partial T^*}{\partial\theta}\cos\theta]\sin\theta = E^2(\zeta r\sin\theta)\end{gathered} \tag{2.23}$$

We will also employ a substitution in eq. 2.23 which will be further elaborated in the next section, we will be substituting the vorticity by modified vorticity F and

G, also, the 'r' will be transformed as r=e^Z where F=$\frac{\zeta}{e^Z sin\theta}$ and G= $\zeta e^Z sin\theta$. The dimensionless energy equations using 2.6,2.7 for particle and fluid are:

$$\nabla^2 T_p^* + Q(r) = 0 \tag{2.24}$$

$$\nabla^2 T_f^* = 2RePr(\mathbf{u}.\nabla)T_f^* \tag{2.25}$$

Special Case 2.1. Now we consider the case when the viscous force are dominating the inertial forces (viscous forces > Inertial forces) and apply the condition that Re→0 in the equations 2.23 2.24 and 2.25 as we are trying to be in line with Stokes derivation. Hence the equations will be reduced to as

$$E^2\psi = \zeta r \sin\theta \tag{2.26}$$

$$-2Gr[\frac{\partial T^*}{\partial r} r \sin\theta + \frac{\partial T^*}{\partial \theta}\cos\theta]\sin\theta = E^2(\zeta r \sin\theta) \tag{2.27}$$

$$\nabla^2 T_p^* + Q(r) = 0 \tag{2.28}$$

$$\nabla^2 T_f^* = 0 \tag{2.29}$$

The Source term will be assumed to be Gaussian and will be of the form as:

$$Q = I_0 \exp(-\frac{r^2}{2\omega_0^2}) \tag{2.30}$$

where I_0 is the beam intensity and ω_0 is the waist of the beam applied.

2.4 Boundary Conditions

The boundary conditions are necessary to solve the eq. 2.23 2.24 2.25 2.26. The boundary conditions should be appropriately defined to yield a reasonable and accurate solution of the problem at hand.

The boundary conditions used in the simulations are as follows:

2.4.1. Sphere Surface

For the momentum equation, the sphere surface is treated with a no-slip conditions which implies that the velocity is zero at the surface when r=A, where "A" is the radius of the sphere.

$$V_r = 0 \ and \ V_\theta = 0 \ ; r = A \ , 0 \leq \theta \leq \pi \tag{2.31}$$

which can be also be interpreted in terms of stream function (ψ) and vorticity (ζ) as:

$$\psi = C' \ and \ \zeta = \frac{E^2\psi}{sin\theta} \ ; r = A \ , 0 \leq \theta \leq \pi \tag{2.32}$$

where C' is a constant.

For the energy equation, as we are solving for fluid as well as solid, The will apply the continuity condition for the fluid as well as the solid,The heat flux boundary condition in case of a thin-cap approximation limit, the thermal conductivity of the cap is not relevant, the condition are as follows:

$$T_s = T_f \ ; r = A \ , 0 \leq \theta \leq \pi \tag{2.33}$$

$$-\partial_r T_f(A, \theta) + -\partial_r T_p(A, \theta) = Q(\theta) \tag{2.34}$$

where Q(θ)=Q for the coated side and Q(θ)=0 for the un-coated side.

2.4.2. Axis of Symmetry

For the momentum equation, along the axis of symmetry, θ= $0/\pi$, the no-cross flow condition applies, which state that the velocity component in angular direction is zero. Hence, the axis of symmetry condition is as follows:

$$V_\theta = 0 \ ; \theta = 0, \ \theta = \pi \tag{2.35}$$

which can be also be interpreted in terms of stream function as:

$$\frac{\partial\psi}{\partial\theta} = \frac{\partial\psi}{\partial r} = 0 \ ; \theta = 0, \ \theta = \pi \tag{2.36}$$

The stream function ψ at the surface and axis of symmetry coincides, so at these point, it is

$$\psi_s = \psi_{\theta=0,\pi} = C'' \tag{2.37}$$

where C'' is a constant.

The vorticity ζ along the axis of symmetry is:

$$\zeta_{\theta=0,\pi} = 0 \tag{2.38}$$

For the energy equation, as the flow is symmetric along the axis and function is a continuous function, Hence:

$$\frac{\partial T}{\partial \theta}_{\theta=0,\pi} = 0 \tag{2.39}$$

2.4.3. Outer Boundary

Far from the sphere, there is undisturbed parallel flow, all the dependent variables reaches an asymptote. The disturbance caused by the sphere is assumed to be non-existent. This condition theoretically is satisfied as r→∞. Computationally, it is not feasible in terms of computation time, storage as well as numerically. it is not realistic to carry out computations on such a large domain, in other cases it is not possible to carry out numerical integration on such large a scale. In other words any boundary condition applied will be an approximation to mimic the behavior to a certain extent. In light of these arguments, the outer boundary condition will be applied at some finite boundary far from the sphere. for the momentum equation.The outer boundary condition in terms of velocity reads:

$$\bar{V} = W(free\ stream\ velocity)\ as\ r \to \infty \tag{2.40}$$

The outer boundary condition for Stream function reads

$$\psi = \frac{W}{2} r^2 \sin^2\theta\ as\ r \to \infty \tag{2.41}$$

The outer boundary condition for vorticity is:

$$\zeta = 0\ as\ r \to \infty \tag{2.42}$$

For the energy equation, the Temperature reaches the ambient temperature but the dimensionless temperature condition reads

$$T_f = 0\ as\ r \to \infty \tag{2.43}$$

2.5 Numerical Technique

The problem at hand can be mathematically modelled by a set of partial differential equations as described in section 2.3. The initial step in solving any the partial differential equation by finite difference method (FDM) is to reduce the differential equations into discrete form and solve the descritized equations using a digital computer. The details can be found in a standard book on numerical analysis.

The most basic and standard method is to expand the terms in Taylor series expansion. The series are then truncated to a reasonable accuracy and the finite difference equations obtained by truncated series substitutions are then solved. The finite difference schemes relates the value of any function at a mesh point with values of function at its neighboring mesh points. The number of neighboring points involved depends on the order of the original differential equation and order of accuracy desired. The FDM scheme will involve more points if more accuracy is desired.

The second-order central finite-difference scheme was utilized in the solving the partial differential equations and obtaining the solution of the equations. The Stream function ψ and vorticity ζ are known to change the most close to the surface of sphere. Hence, the The transformation r=e^Z was employed in the equations described in section 2.3 to cater for this phenomenon with equal intervals in Z,where F=$\frac{\zeta}{e^Z sin\theta}$ and G= $\zeta e^Z sin\theta$..

The equations eq. 2.23 2.24 2.25 2.26 in transformed coordinated are:

$$e^{2Z}E^2\psi - \zeta e^{3Z}\sin\theta = 0 \tag{2.44}$$

$$\begin{gathered}\frac{Re}{2}\left[\frac{\partial\psi}{\partial Z}\cdot\frac{\partial F}{\partial\theta} - \frac{\partial\psi}{\partial\theta}\cdot\frac{\partial F}{\partial Z}\right]e^Z\sin\theta - \\ 2Gr[\frac{\partial T^*}{\partial Z}\sin\theta + \frac{\partial T^*}{\partial\theta}\cos\theta]e^{2Z}\sin\theta - e^{2Z}E^2(G) = 0\end{gathered} \tag{2.45}$$

$$\frac{\partial^2 T_p^*}{\partial^2 Z} + \frac{\partial T_p^*}{\partial Z} + \frac{\partial^2 T_p^*}{\partial^2\theta} + \cot\theta\frac{\partial T_p^*}{\partial\theta} + e^{2Z}Q = 0 \tag{2.46}$$

$$\frac{\partial^2 T_f^*}{\partial^2 Z} + \frac{\partial T_f^*}{\partial Z} + \frac{\partial^2 T_f^*}{\partial^2\theta} + \cot\theta\frac{\partial T_f^*}{\partial\theta} - \frac{2RePr}{e^Z\sin\theta}[\frac{\partial\psi}{\partial Z}\cdot\frac{\partial T_f^*}{\partial\theta} - \frac{\partial\psi}{\partial\theta}\cdot\frac{\partial T_f^*}{\partial\zeta}] = 0 \tag{2.47}$$

where,

$$e^{2Z}E^2 = \frac{\partial^2}{\partial^2 Z} - \frac{\partial}{\partial Z} + \sin\theta\frac{\partial}{\partial\theta}(\frac{1}{\sin\theta}\frac{\partial}{\partial\theta}) \tag{2.48}$$

The second order central difference formulation was utilized to solve the eqs 2.44, 2.45, 2.46 and 2.47.

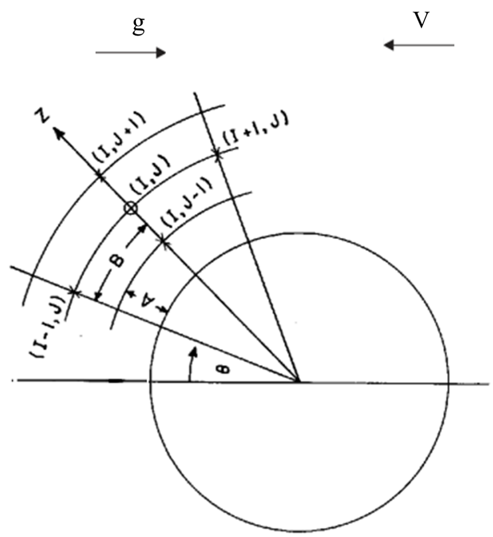

Figure 2.2: Circular Mesh System.

The circular-mesh system was used to solve the system, as shown in fig 2.2. The lattice size 'A' is in Z direction while the 'B' was utilized in the θ direction. The first argument 'I' corresponds to the angle θ displacement while the second argument 'J' corresponds to displacement in 'Z' direction. The second-order central finite difference scheme for a a general variable ' f' is shown as:

$$f^{'}(x) = \frac{f(x+h) - f(x-h)}{2h} \tag{2.49}$$

$$f^{''}(x) = \frac{f(x+h) - 2f(x) + f(x-h)}{h^2} \tag{2.50}$$

The forward and backward finite difference scheme for a general variable 'f' are given as, which were used for end nodes:

$$f^{'}(x) = \frac{f(x+h) - f(x)}{h} \tag{2.51}$$

$$f^{'}(x) = \frac{f(x) - f(x-h)}{h} \tag{2.52}$$

The vorticity ζ condition for the sphere surface is a bit tricky and hence is elaborated for clarity, the boundary condition in finite difference form is:

$$\zeta(I,1) = \frac{8\psi(I,2) - \psi(I,3) - 7\psi(I,1)}{2A^2 \sin\theta(I)} \tag{2.53}$$

The relaxation factor were utilized in the current iterative procedure to stabilize as well as to accelerate the computations. They were used for stream function ψ, Vorticity ζ, Modified Vorticity G, and Temperature (T_p and T_f).The relaxation equations are same for each dependent variable. They are introduced as:

$$\psi_n(I,J) = \psi_{n-1}(I,J) + W_1\left[\psi_n^*(I,J) - \psi_{n-1}(I,J)\right] \tag{2.54}$$

$$\zeta_n(I,J) = \zeta_{n-1}(I,J) + W_2\left[\zeta_n^*(I,J) - \zeta_{n-1}(I,J)\right] \tag{2.55}$$

$$G_n(I,J) = G_{n-1}(I,J) + W_3\left[G_n^*(I,J) - G_{n-1}(I,J)\right] \tag{2.56}$$

$$(T_p^*)_n(I,J) = (T_p^*)_{n-1}(I,J) + W_4\left[(T_p^*)_n^*(I,J) - (T_p^*)_{n-1}(I,J)\right] \tag{2.57}$$

$$(T_f^*)_n(I,J) = (T_f^*)_{n-1}(I,J) + W_5\left[(T_f^*)_n^*(I,J) - (T_f^*)_{n-1}(I,J)\right] \tag{2.58}$$

Where $W_1 - W_5$ represents the relaxation factors used for each dependent variable. The 'n' stands for the n^{th} value calculated in the iterative procedure, while $*$ stands for the values of dependent variables calculated using the eqs 2.44, 2.45, 2.46 and 2.47.

The iterative procedure were carried out to achieve an accuracy of less than $1e^{-4}$.

2.6 Mesh Independence

The mesh independence was carried out for reference case similar to [21] at Reynolds number of 5 and a domain size of R=6 or Z=1.8. The δr='A' (radial step size) and $\delta\theta$='B' (angular step size) was checked for a range of 0.2-0.025 and 12-1 (deg) respectively. The simulations became independent at A=0.05 and B=1^o as shown in fig 2.3 and fig 2.4 respectively.

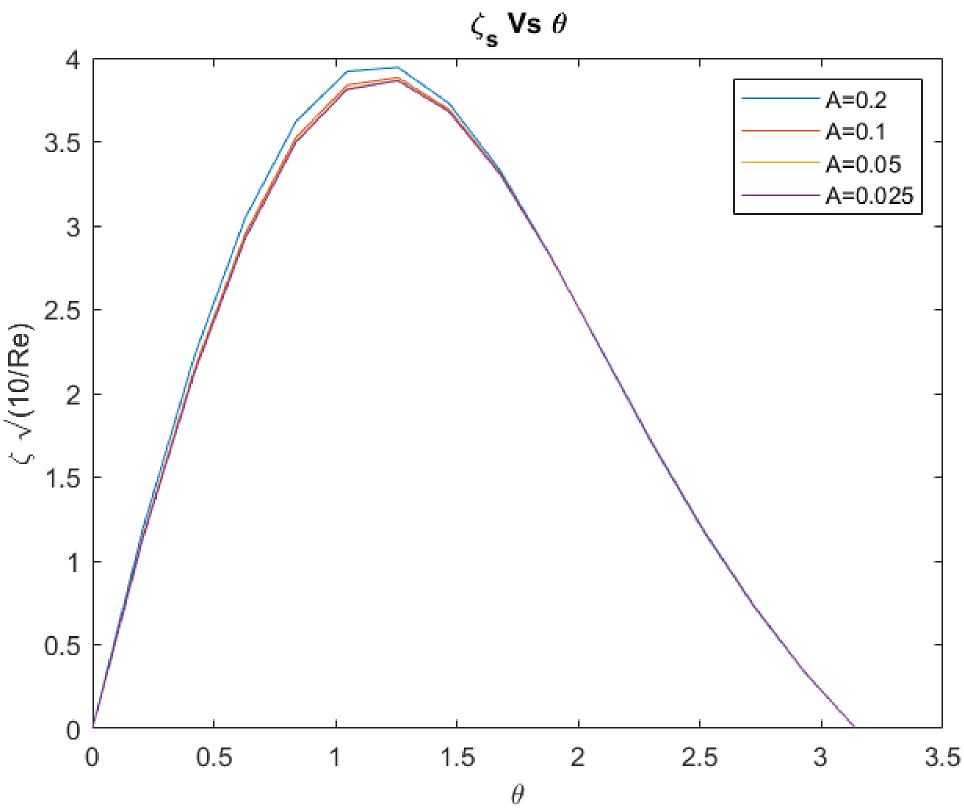

Figure 2.3: Mesh Independence in 'A'.

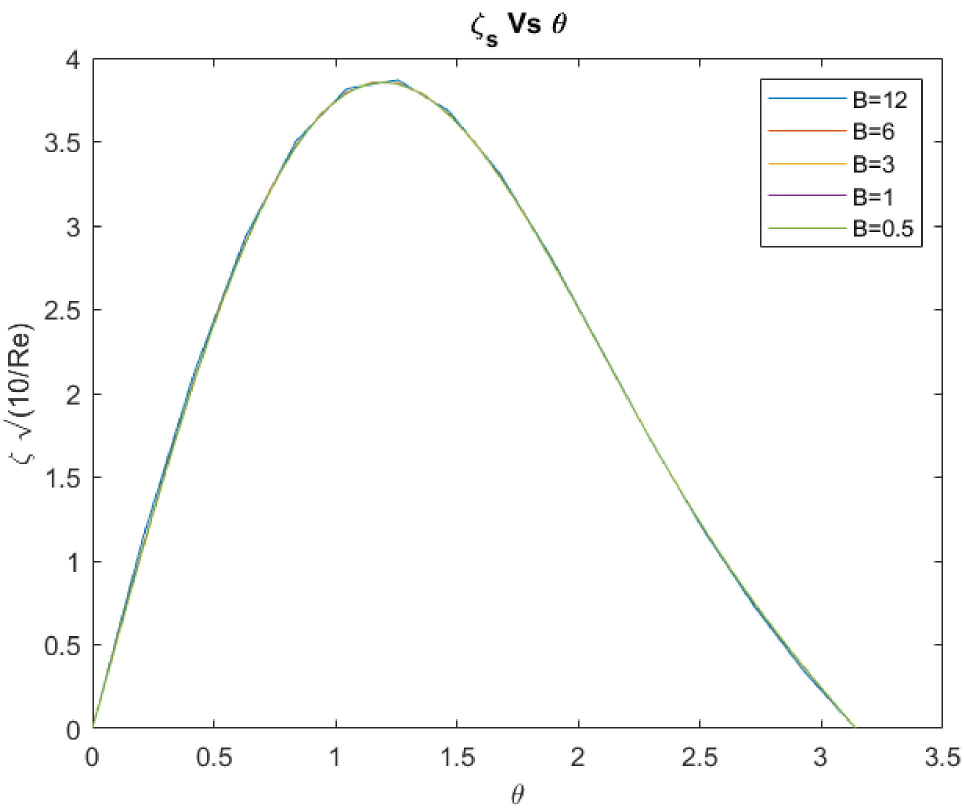

Figure 2.4: Mesh Independence in 'B'.

2.7 Validation

The Validation was carried out with [21]. The Reynold number for the validation case was 5 and he considered a domain size of Z=1.8 or R=6.

Table 2.1: Result Comparison.

Results	Re	Z	Cd_f	Cd_p	Cd_{total}
Jenson [21]	5	1.8	5.34	2.65	8.03
BIL-FLOW	5	1.8	5.26	3.95	9.22
Hamielec [19]	0.1	2.9497	-	-	262
Experimental [19]	0.1	2.9497	-	-	240
BIL-FLOW	0.1	2.9497	-	-	208.06
Hamielec [19]	1.0	1.9459	-	-	32.5
Experimental [19]	1.0	1.9459	-	-	26.5
BIL-FLOW	1.0	1.9459	-	-	28.87

The results are in good agreement with [21] [21] as shown in fig 2.5 and table 2.1. The error reason as [21], [19] used a larger step size as compared to present results. The error can be contributed by the digital computers of his era as the machines of that time might not being considering more decimal place as compared to the computers of current era, when the step size as used by [21] was utilized the results were in good agreement.

2.8 Simulations

The numerical simulations were carried out with variation of Grashoff number (0.1-1.5) and varying the intensity (1-10) and waist (0.1-0.75) of the Gaussian beam at Re $\rightarrow$0. The Gaussian beam applied is acting only on one half of the particle and it is switched off on other part of the particle.

The Gaussian profile is of the form as shown in fig. 2.7 for a Janus particle. The Janus particle will be studied for two configuration, Janus sphere cap-up and Janus sphere cap-down, along gravity and opposite to gravity respectively.

Drag Calculations:

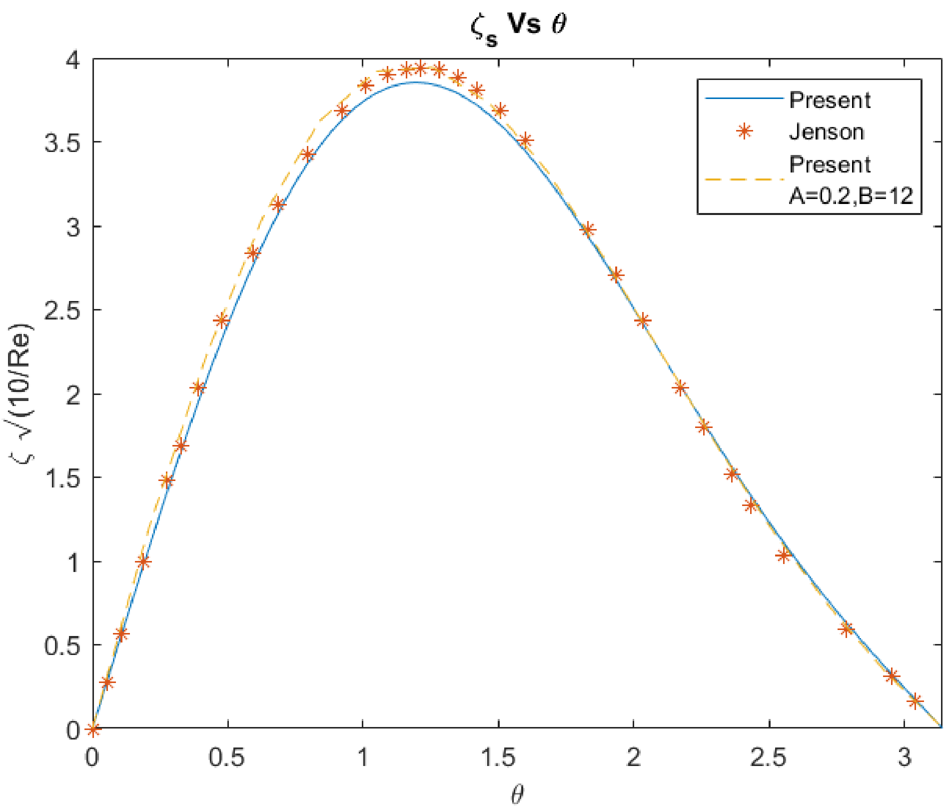

Figure 2.5: Validation Case with Step Size.

Consider the non-dimensionalised form of the equation with condition Re→0

$$\nabla P^* = \nabla^2 U^* - GrT^* \tag{2.59}$$

Now, consider the component of pressure in radial direction, we will have:

$$\frac{\partial P^*}{\partial r} = -\frac{1}{r^2 sin\theta}\frac{\partial}{\partial\theta}(E^2\psi) + GrT^*\cos\theta \tag{2.60}$$

using 2.26 and after simplification:

$$\frac{\partial P^*}{\partial r} = -\frac{2}{r}\frac{\partial\zeta}{\partial\theta} + GrT^*\cos\theta \tag{2.61}$$

After integrating we obtain pressure at front stagnation point as:

$$P_0^* = 2\int_1^\infty \frac{\partial\zeta}{\partial\theta}dZ + Gr\int_1^\infty T^* e^Z \cos\theta dZ \tag{2.62}$$

Similarly for the θ component the pressure as a function of angle would come out to be:

$$P^* = P_0^* + \int_0^\theta (\frac{\partial\zeta}{\partial Z} + \zeta)d\theta - Gr\int_0^\theta T^*\sin\theta d\theta \tag{2.63}$$

$$C_{DP} = \frac{D_P}{\pi R^2 \times \frac{1}{2}\frac{\rho_\infty \nu_\infty^2}{R^2}} \tag{2.64}$$

where,

$$D_P = \iint_S P\sin\beta dS$$

Hence,

$$c_{DP} = \int_0^\pi P_\Theta \sin 2\theta d\theta \tag{2.65}$$

The viscous drag coefficient is:

$$C_{DF} = \frac{D_F}{\pi R^2 \times \frac{1}{2}\frac{\rho_\infty \nu_\infty^2}{R^2}} \tag{2.66}$$

where,

$$D_F = \iint_S \tau_{r\Theta} \cos\beta dS$$

Hence,

$$C_{DF} = 4\int_0^\pi \zeta_S^* \sin^2\Theta d\theta \tag{2.67}$$

The cap-up and cap-down configuration is shown in fig.2.6 for clarity.

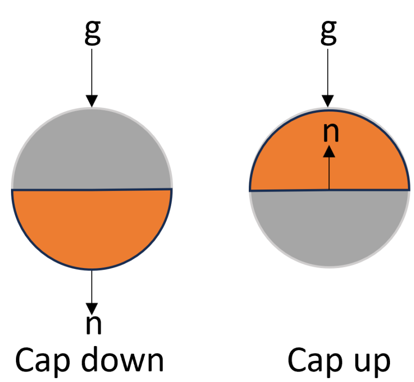

Figure 2.6: Cap-down and cap-up configuration for a Janus Sphere.

2.8.1. Janus Cap-down

The Janus Particle with cap down configuration was studied with the variation in Grashoff number, Intensity and waist of the beam. The Janus with Cap-down refers to the configuration in which the normal vector pointing at the coated side is pointing parallel to the direction of gravity. The surface vorticity results are shown in figure 2.8, 2.9 and 2.10. As per the vorticity results, the vorticity is not effected much if the waist of the beam is very small but with the increase in waist, when the Grashoff and intensity is increased. the surface vorticity is also shifted

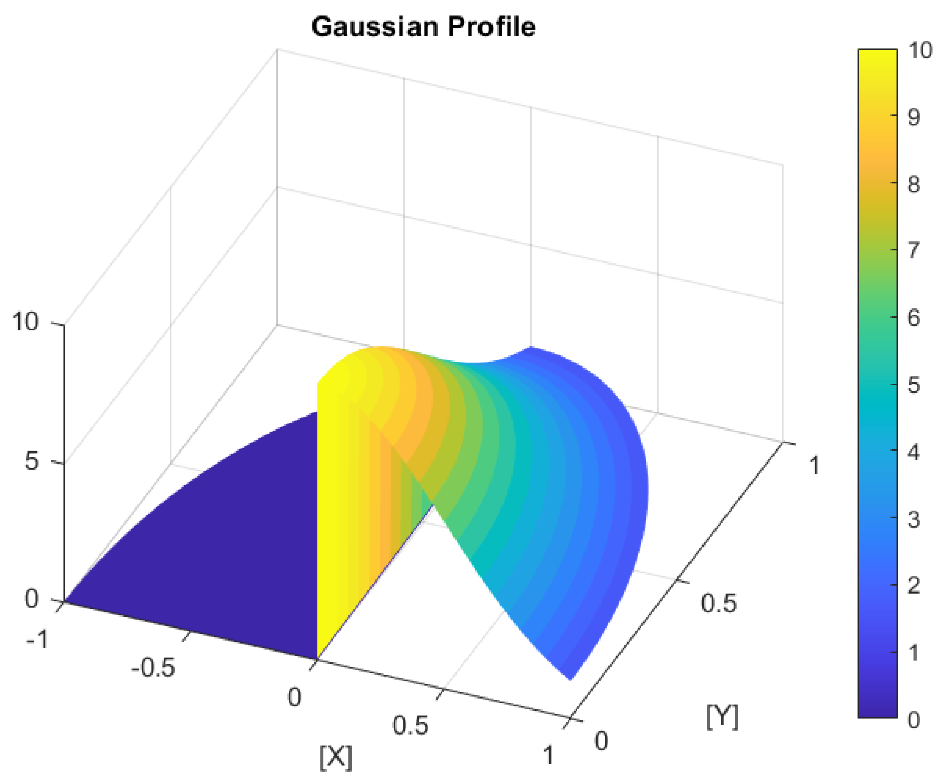

Figure 2.7: Gaussian Heating Potential for a Janus Sphere.

towards the non-capped side of the sphere and this effect is more prominent at higher Grashoff with bigger waist and larger intensity value.

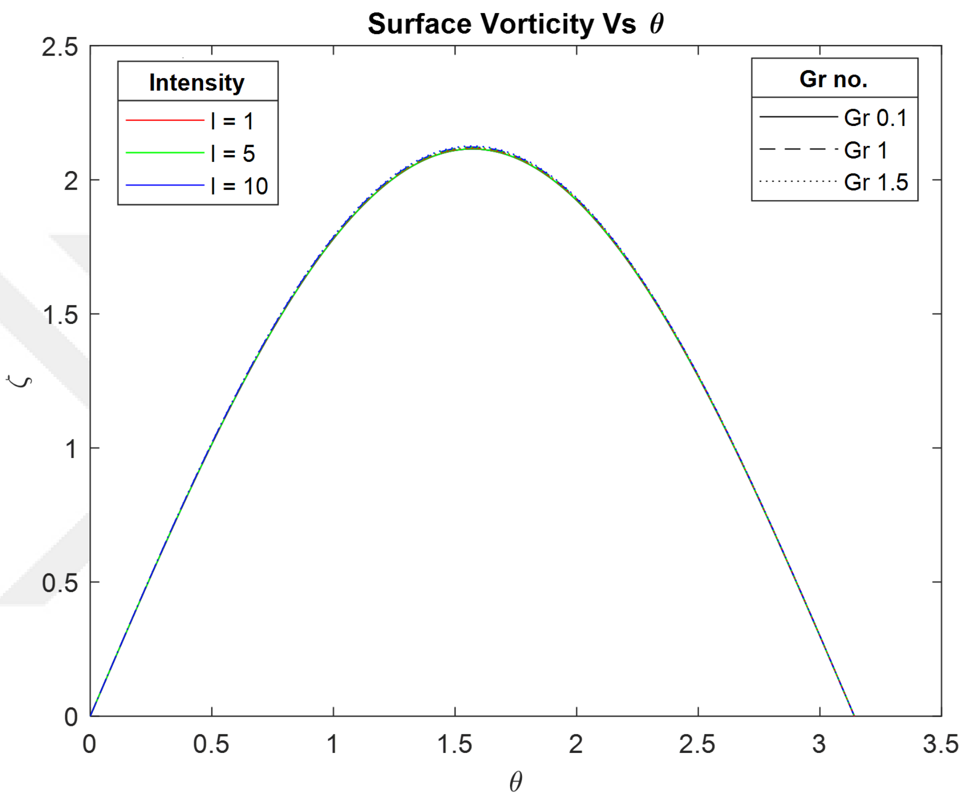

Figure 2.8: Surface Vorticity at waist of 0.1[Cap Down].

Drag Coefficients

The Coefficient of drag are shown in figure 2.11 and 2.12. The Drag Coefficient showed that with the increase in Grashoff, the frictional drag coefficient and Pressure drag coefficient increase almost linearly. The increase is substantial at higher intensity and waist but almost negligible at very low intensity and waist of the applied beam. The frictional drag is effected more as compared to pressure drag.

2.8.2. Janus Cap-up

The Janus Particle with cap down configuration was studied with the variation in Grashoff number, Intensity and waist of the beam. The Janus with Cap-down refers to the configuration in which the normal vector pointing at the coated side is pointing in the direction opposite to the direction of gravity. The surface vorticity

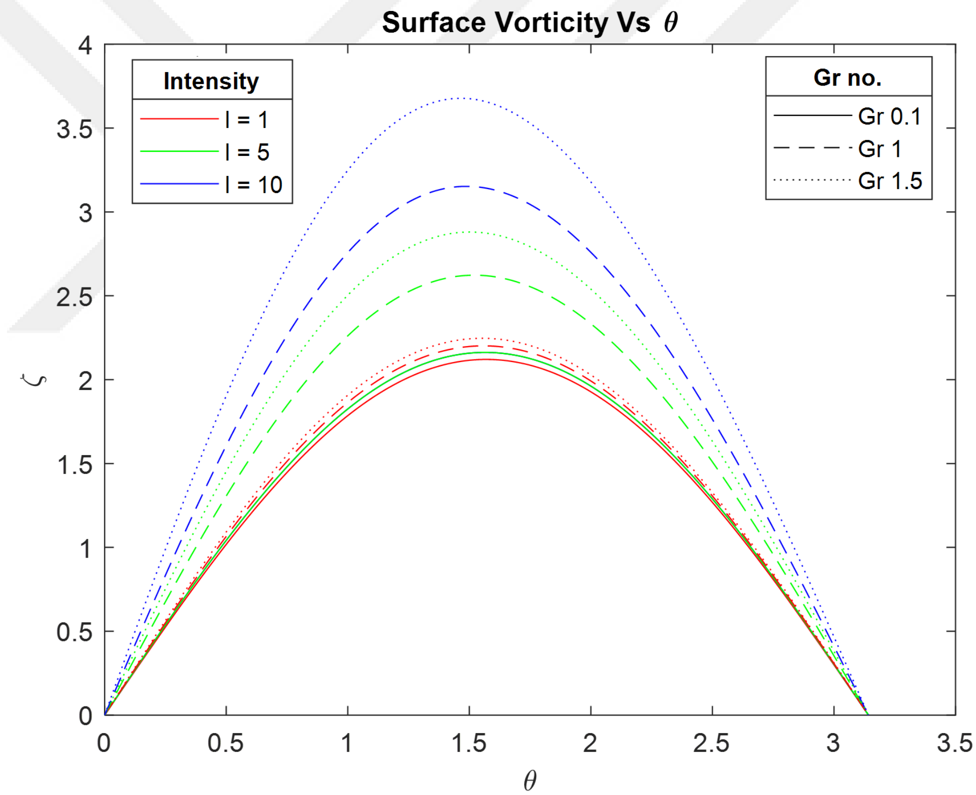

Figure 2.9: Surface Vorticity at waist of 0.5[Cap Down].

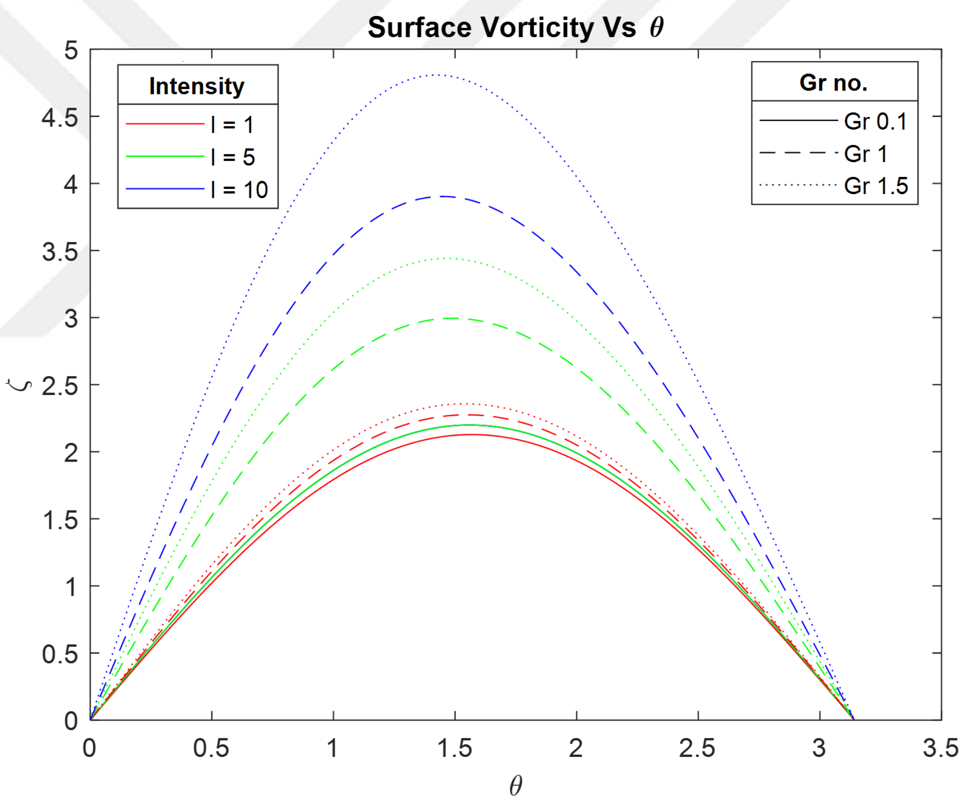

Figure 2.10: Surface Vorticity at waist of 0.75[Cap Down].

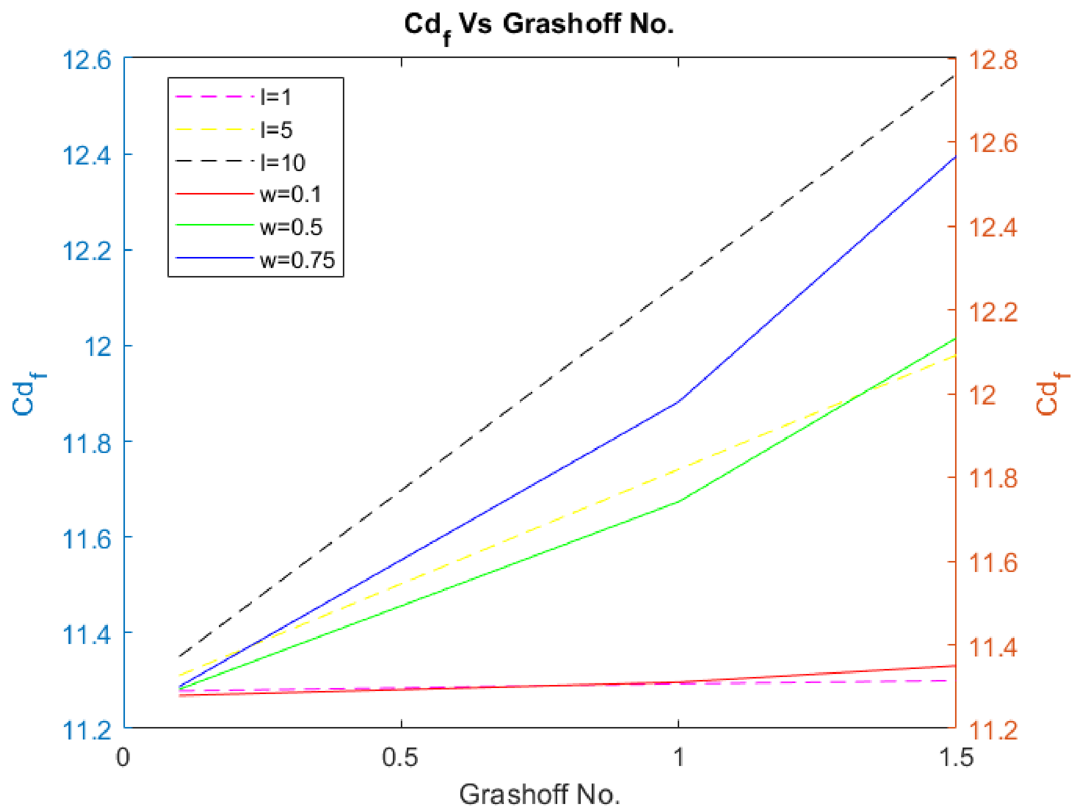

Figure 2.11: Coefficient of Drag (frictional) Vs Grashoff No[Cap Down].

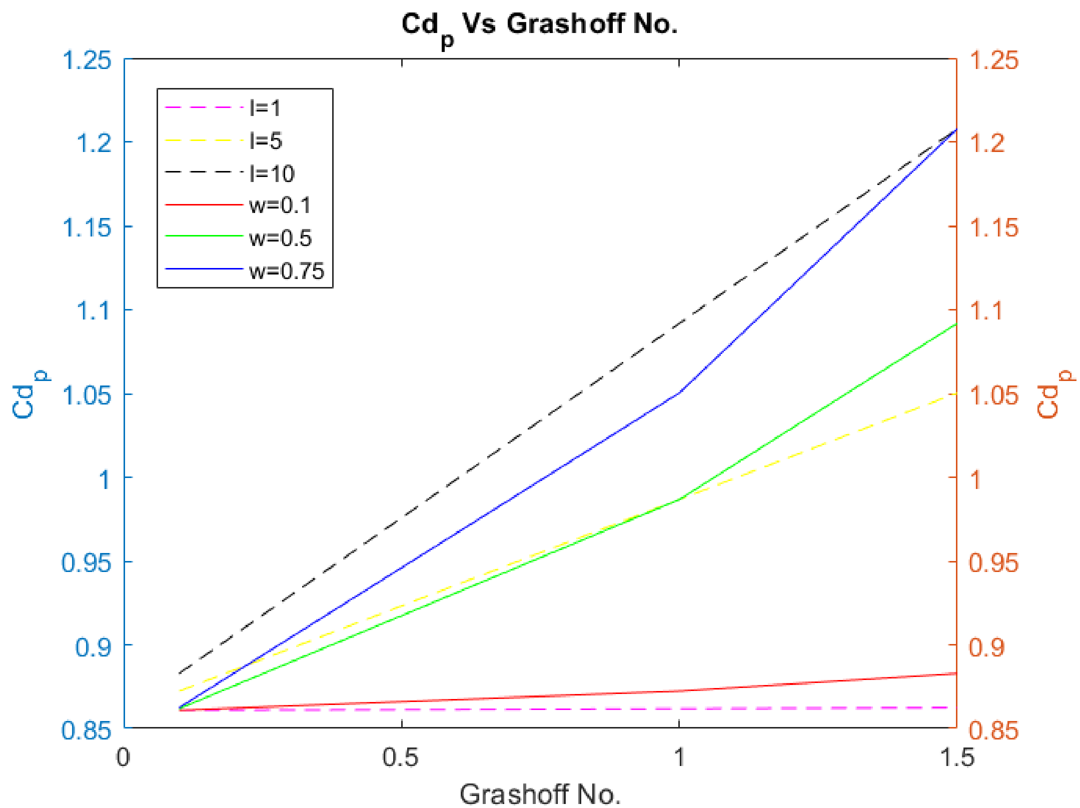

Figure 2.12: Coefficient of Drag (Pressure) Vs Grashoff No[Cap Down].

results are shown in figure 2.13, 2.14 and 2.15. Similar to cap-up configuration.As per the vorticity results, the vorticity is not effected much if the waist of the beam is very small but with the increase in waist, when the Grashoff and intensity is increased surface vorticity is increased. the surface vorticty is also shifted towards the non-capped side of the sphere and this effect is more prominent at higher Grashoff with bigger waist and larger intensity value.

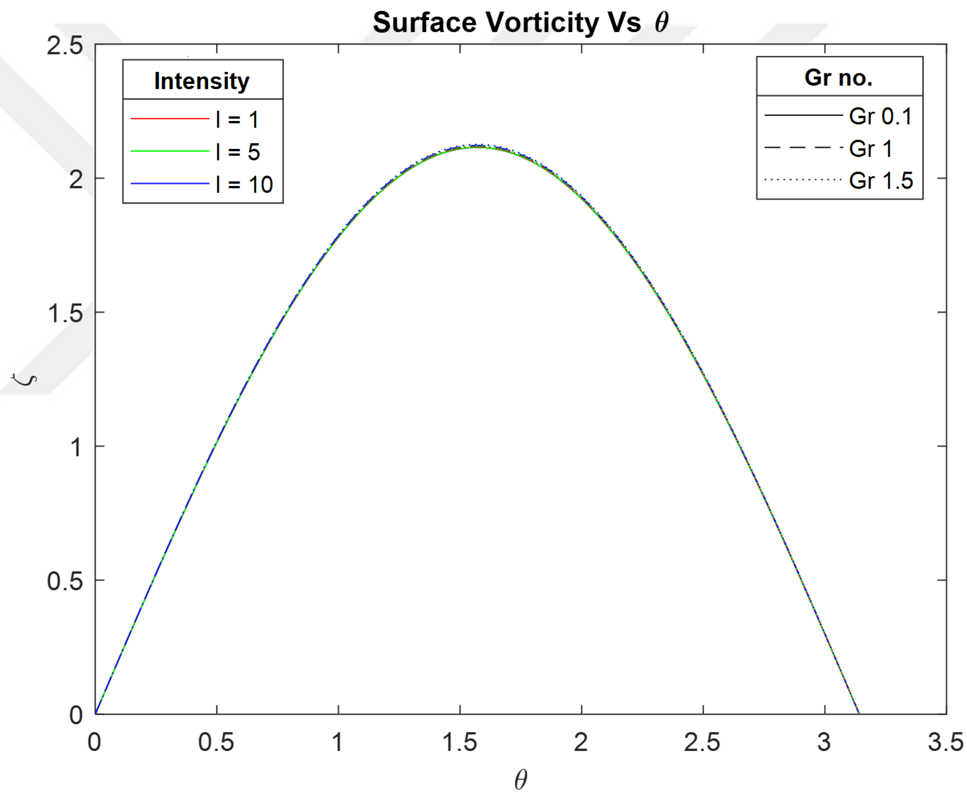

Figure 2.13: Surface Vorticity at waist of 0.1[Cap Up].

Drag Coefficients

The Coefficient of drag are shown in figure 2.16 and 2.17. The Drag Coefficient showed that with the increase in Grashoff, the frictional drag coefficient increase linearly with Grashoff number and the increase is substantial at higher at higher intensity and waist of the beam while Pressure drag coefficient decrease almost linearly and the increase is substantial at higher intensity and waist but almost negligible at very low intensity and waist of the applied beam. The frictional drag is effected more as compared to pressure drag.

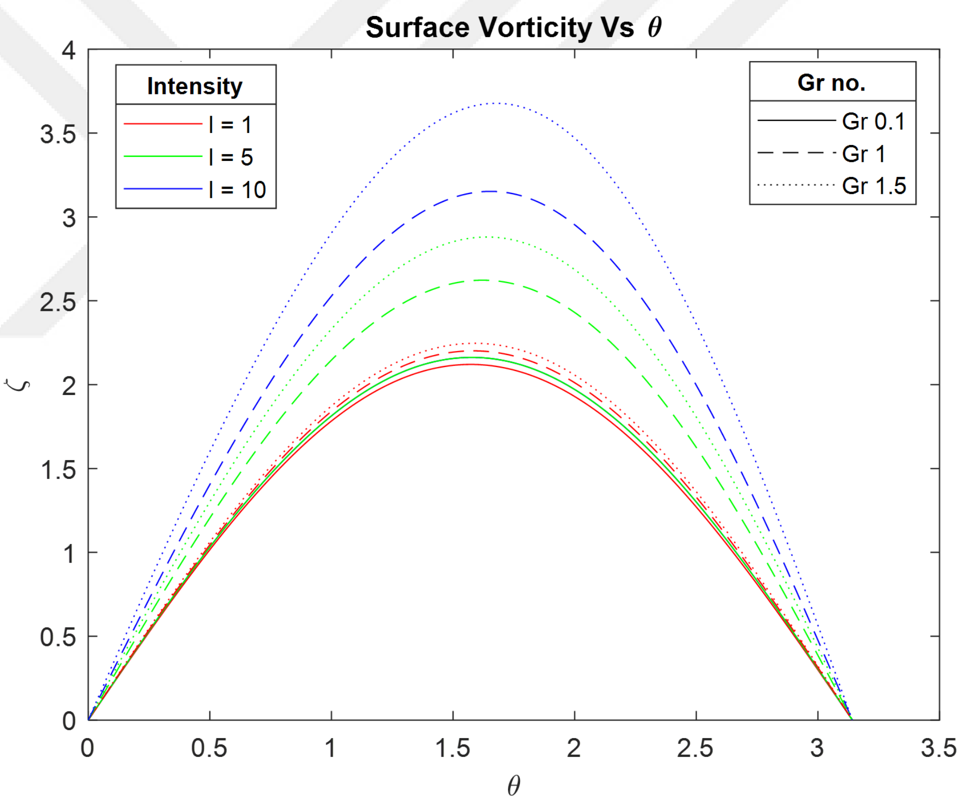

Figure 2.14: Surface Vorticity at waist of 0.5[Cap Up].

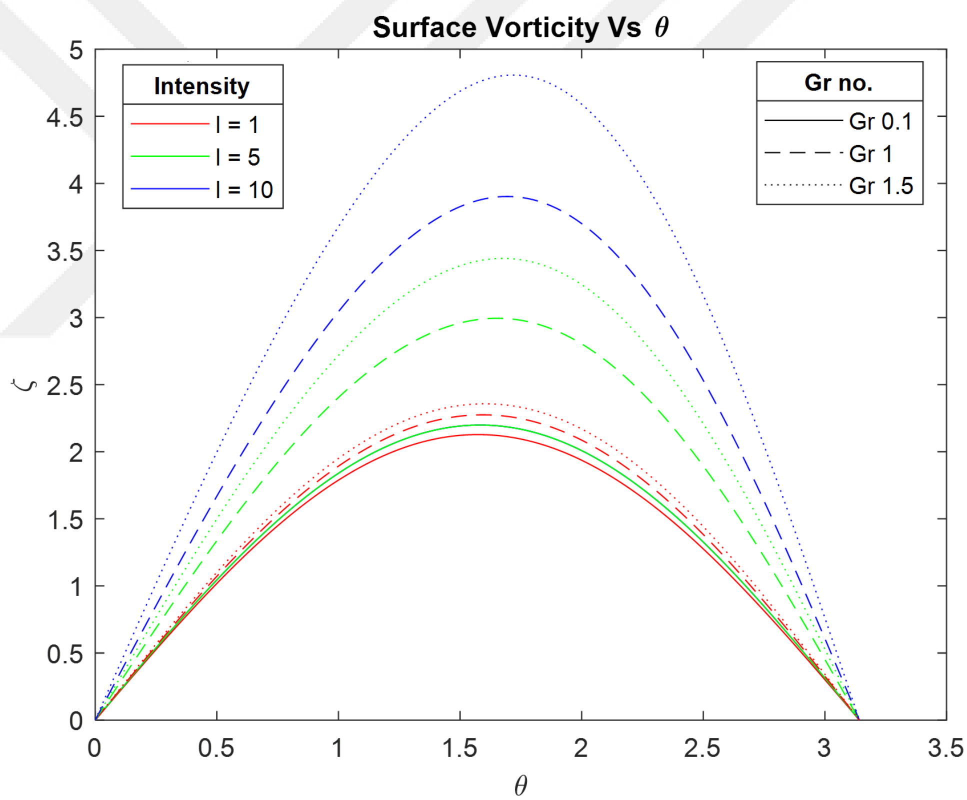

Figure 2.15: Surface Vorticity at waist of 0.75[Cap Up].

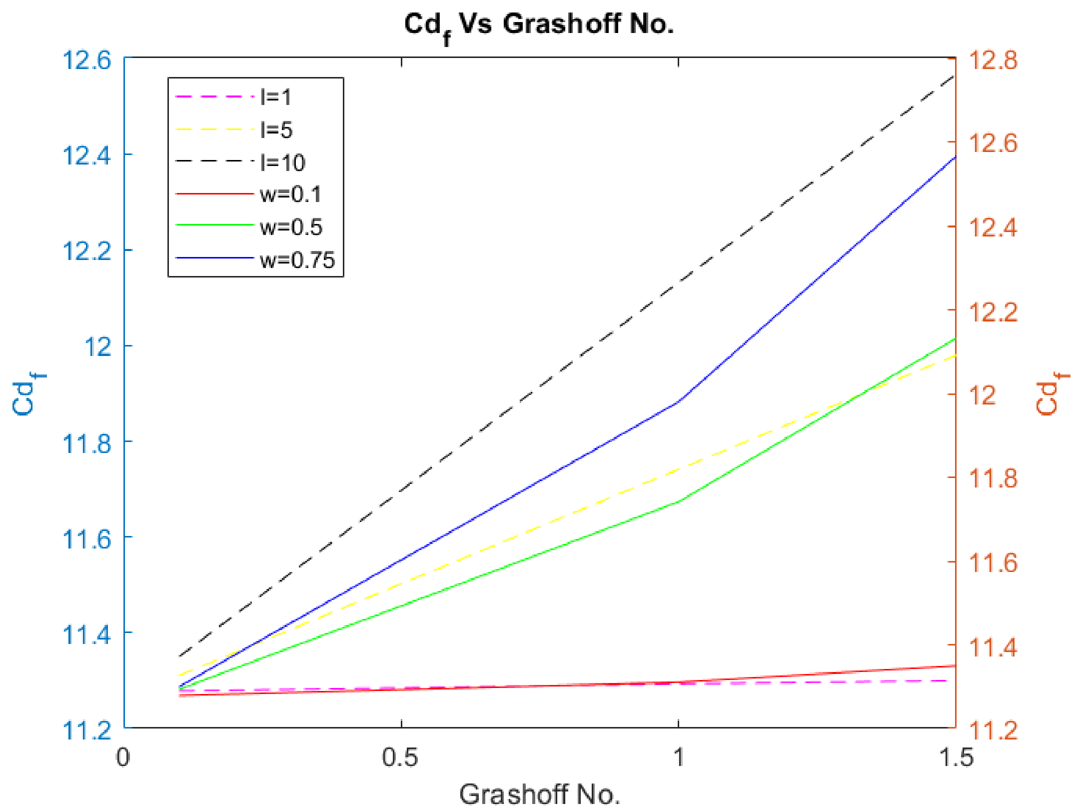

Figure 2.16: Coefficient of Drag (frictional) Vs Grashoff No [Cap Up].

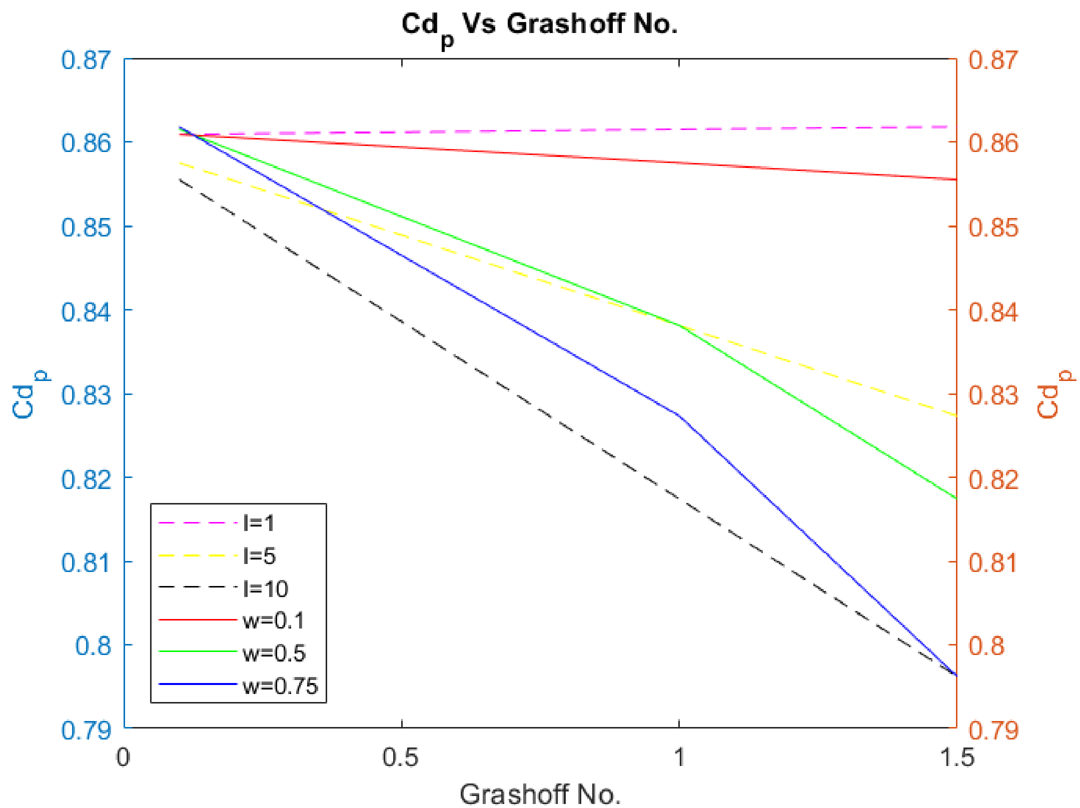

Figure 2.17: Coefficient of Drag (Pressure) Vs Grashoff No[Cap Up].

2.8.3. Slip and Phoretic Velocity

The slip velocity and translational velocity can be calculated using the relationship

$$v_s = \mu \nabla T_{||}$$

$$\boldsymbol{u} = -\frac{1}{|\mathcal{S}|} \oint_{\mathcal{S}} \mathrm{d}S \boldsymbol{v}_{\mathbf{s}} = -\frac{1}{4\pi} \int_0^{2\pi} \mathrm{d}\phi \int_0^{\pi} \mathrm{d}\theta \sin\theta \boldsymbol{v}_{\mathbf{s}}$$

The results are given for minimum (Gr=0.1, I=1, Waist=0.1) and maximum case (Gr=1.5, I=10, Waist=0.75) as in figure 2.18 and 2.19 respectively. The slip and phoretic translational velocity is greatly increased though in cap up configuration the slip and phoretic translational velocity is greater than slip and phoretic translational velocity in cap down configuration.

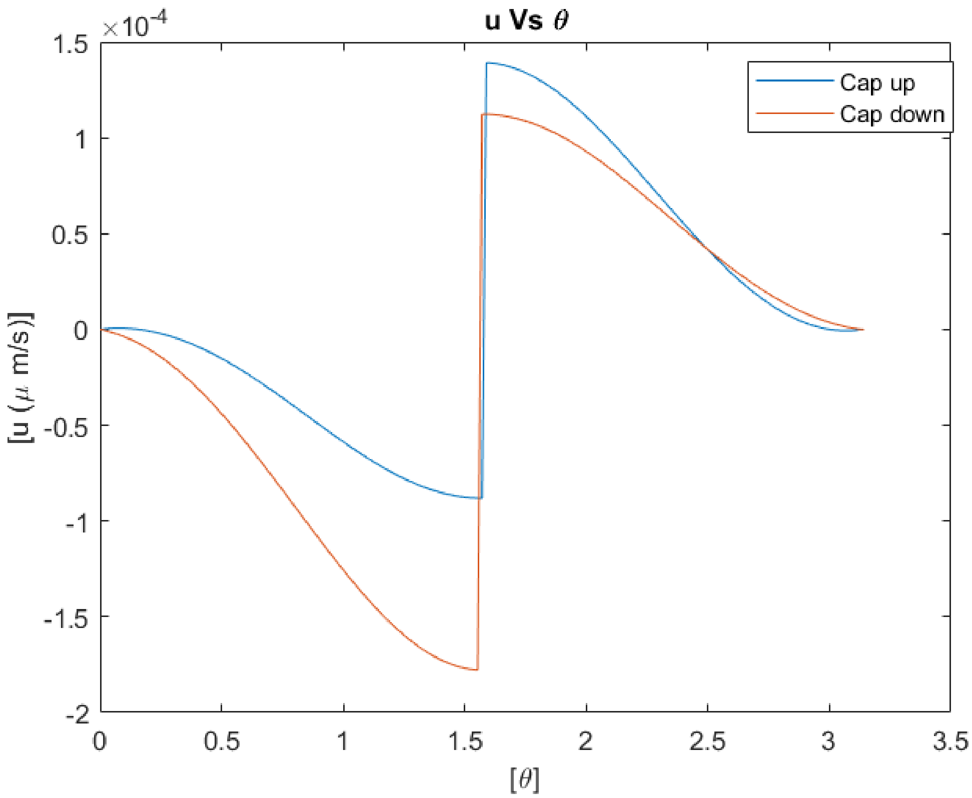

Figure 2.18: Slip velocity Vs Theta Case Min.

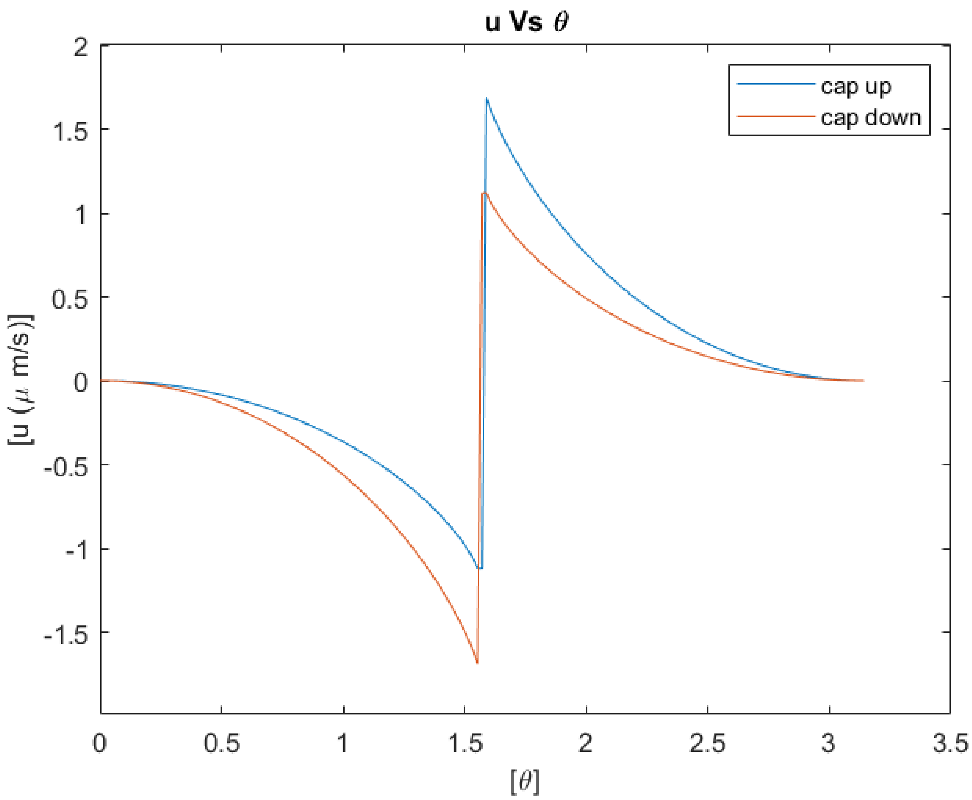

Figure 2.19: Slip velocity Vs Theta Case Max.

2.9 Summary

In this chapter, we developed a BIL-Flow, an in-house code for fluid flow over a Janus sphere using the stream function-vorticity approach, which can be used to study the effect of Gaussian heating on a Janus particle and fluid around. The effect of Grashoff number, beam intensity and Beam waist was studied.Additionally, self thermophoretic velocity as well as drag of Janus sphere was calculated. As per the study. The vorticity is enhanced with increasing Grashoff number but the intensity and waist act as a mediator which further increase the thermal effects. To conclude, the thermal effect in case of Janus sphere (acting as a heat source) in a fluid is non-negligible and essential.

Chapter 3

Modelling Optical Tweezers in an Optical Potential

3.1 Introduction

In Chapter 2, we developed a numerical mode which will help us to study and understand flow behavior near an activated Janus particle as well as to calculate drag and self-thermophoretic velocity around the Janus sphere. The effect on a particle caused by the application of an optical potential needs to be studied.
The study of optical tweezers is of importance as they have wide spread uses in fields from biology to physics [22–28]. The optical tweezers have been slowly and steadily consolidating their importance in many fields.The optical tweezers were invented in 1986 [29]. The optical tweezers is the term used for optical manipulation of particle under the influence of a tightly focused laser beam.

The Geometric Ray Approximation of light is valid when the wavelength of light is comparable or bigger then the size of the particle usually the particle size is R$\geq$1μm, if the particle size is smaller than the wavelength (λ) then the Mie-Theory or Dipole approximation will have to be applied as Geometric Ray Approximation becomes invalid [30].

In this chapter, we will develop and validate BIL-OP ,an in-house code, which will be used to calculate forces and torque on a micro-particle under an optical potential utilizing the Geometric Ray Approximation.
This chapter is independent and self-contained and the reader will not have to refer to Ch2 and Ch4 to understand Geometric Ray Approximation.Hence, the reader can be at ease and avoid any confusion.

3.1.1 Notations

The notation $\boldsymbol{P}$ was used to denote the power of the beam with subscript $\boldsymbol{i}$,$\boldsymbol{r}$,$\boldsymbol{t}$ denoting incidence, reflectance and transmittance. $\boldsymbol{r_i}$ represents the incident ray, $\boldsymbol{r_r}$ represents the reflected ray and $\boldsymbol{r_t}$ represents the refracted ray.$\boldsymbol{S}$ represents a surface, $\boldsymbol{S_n}$ represents the normal of the surface under consideration $\|.\|$ represents the magnitude of the vector. The 'Pol' represents the polarization of the beam. θ_C and θ_B represent the critical and Brewster angle respectively.$\sum$ represents the summation and $|.|$ represents the absolute value.

3.2 Problem Statement

To model the effect of optical potential (Optical Beam i.e. Gaussian beam, LG beam etc) on a dielectric particle. The modelling of beam would be carried out by defining beams as rays as per the Geometric ray approximation. The beam would be assumed to be passing through a iris and an objective lens which will focus the beam. Considering the Snell's law, The transmitted and refracted rays will be calculated coupled with Fresnel's equations to account for the effect of polarization resulting in an optical package BIL-OP.

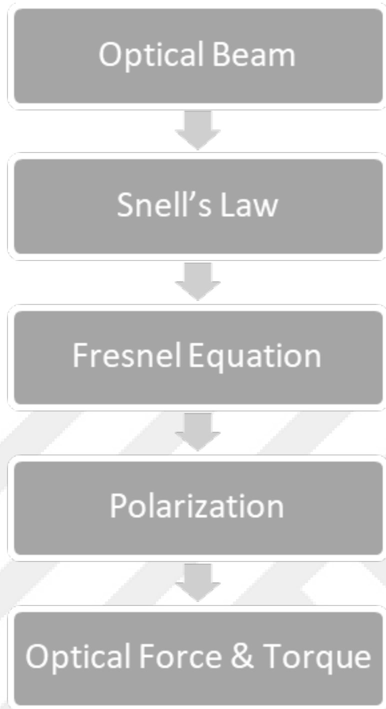

Figure 3.1: Optical Package.

3.3 Modelling of Geometric Ray Approximation

Under the Geometric Ray Approximation, a beam of power ($\boldsymbol{P}$) of light is assumed to be consisting of a number of individual rays, whose cumulative power is equal to the power of the beam applied.for simplicity, consider only a single ray ($\boldsymbol{r_i}$) travelling in a medium of refractive index (n_i) with power ($\boldsymbol{P}_i$), it is striking a surface $\boldsymbol{S}$ with an angle (θ_i), part of the ray power ($\boldsymbol{P_r}$) will be reflected in the direction ($\boldsymbol{r_r}$) and while the other part ($\boldsymbol{P_t}$) will be transmitted in the direction of ($\boldsymbol{r_t}$) into another medium with an refractive index (n_m) with an angle of (θ_t).

The first step is to calculate the incident angle (with reference to surface normal $\boldsymbol{S_n}$) θ_i with known refractive index of the incident medium n_i, This was achieved by defining the starting point (usually away from the beam) and the direction of the beam (beam is applied in the Z direction). The next step is to calculate the point of intersection of the incident ray $\boldsymbol{r_i}$ and the surface $\boldsymbol{S}$, this will help us to obtain θ_i. After calculating θ_i, next variable to be calculated is θ_r, $\boldsymbol{r_r}$ and $\boldsymbol{r_t}$ with known n_m. This is achieved by using Snell's law. the author used the vectorial form of Snell's law to calculate the unknown variables as it can help in avoiding the long and tedious transformations to use the planar form of Snell's law. The Snell's law applied for the problem is:

$$n_i(\boldsymbol{\hat{r}_i} \times \boldsymbol{\hat{S}_n}) = n_m(\boldsymbol{\hat{r}_t} \times \boldsymbol{\hat{S}_n}), \tag{3.1a}$$

$$\theta_r = \theta_t, \tag{3.1b}$$

$$\boldsymbol{\hat{S}_n} \times \boldsymbol{\hat{r}_i} = \|\boldsymbol{\hat{S}_n}\|\|\boldsymbol{\hat{r}_i}\| \sin\theta_i \hat{\eta} \tag{3.1c}$$

$$-\boldsymbol{\hat{S}_n} \cdot \boldsymbol{\hat{r}_t} = \|\boldsymbol{\hat{S}_n}\|\|\boldsymbol{\hat{r}_t}\| \cos\theta_t \tag{3.1d}$$

The problem at hand has less variables and more equations. The row reduced echelon form was used to find the equation with no dependence and the last row (zeros) was substituted with condition 3.1d. This method was applied at each intersection to find the direction and angle of rays. Now, power distribution at each intersection should be calculated with the polarization. in the absence of polarization in light. The amount of power distributed at each reflection and refraction event is obtained through Fresnel Coefficients. By the conservation of energy

$$\boldsymbol{P_i} = \boldsymbol{P_r} + \boldsymbol{P_t} \tag{3.2}$$

For S-polarized light (light electric field vector is perpendicular to incident plane). The reflection and transmission coefficients are:

$$R_s = \left|\frac{n_\mathrm{i}\cos\theta_\mathrm{i} - n_\mathrm{t}\cos\theta_\mathrm{t}}{n_\mathrm{i}\cos\theta_\mathrm{i} + n_\mathrm{t}\cos\theta_\mathrm{t}}\right|^2 \tag{3.3a}$$

$$T_s = \frac{4n_\mathrm{i}n_\mathrm{t}\cos\theta_\mathrm{i}\cos\theta_\mathrm{t}}{|n_\mathrm{i}\cos\theta_\mathrm{i} + n_\mathrm{t}\cos\theta_\mathrm{t}|^2} \tag{3.3b}$$

For P-polarized light (light electric field vector is parallel to incident plane). The reflection and transmission coefficients are:

$$R_p = \left|\frac{n_\mathrm{i}\cos\theta_\mathrm{t} - n_\mathrm{t}\cos\theta_\mathrm{i}}{n_\mathrm{i}\cos\theta_\mathrm{t} + n_\mathrm{t}\cos\theta_\mathrm{i}}\right|^2 \tag{3.4a}$$

$$T_p = \frac{4n_\mathrm{i}n_\mathrm{t}\cos\theta_\mathrm{i}\cos\theta_\mathrm{t}}{|n_\mathrm{i}\cos\theta_\mathrm{t} + n_\mathrm{t}\cos\theta_\mathrm{i}|^2} \tag{3.4b}$$

Also, by conservation of energy:

$$R_s + T_s = 1 \tag{3.5a}$$

$$R_p + T_p = 1 \tag{3.5b}$$

for the circularly or unpolarized light, The average of3.3 3.4 can be used as:

$$R = \frac{R_s + R_p}{2} \tag{3.6a}$$

$$T = \frac{T_s + T_p}{2} \tag{3.6b}$$

They are calculated and shown in fig 3.2 and 3.3:

The coefficient calculation are planar. The polarisation ray tracing matrix was employed to cater for the effect of polarization which involves transformation between the global coordinates in which the 'Pol' is defined and local coordinates at each interface. we employed separate change of basis vector before and after

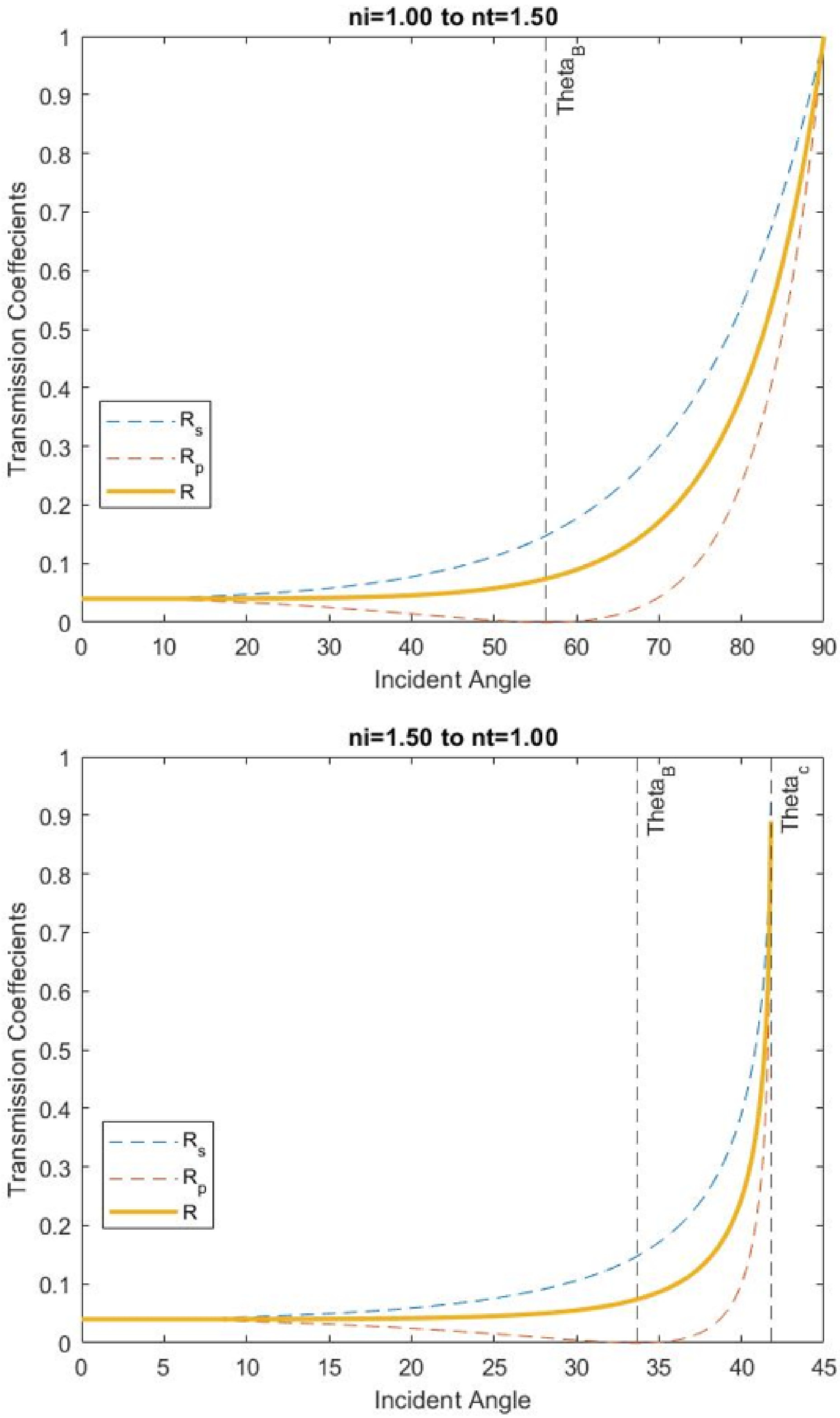

Figure 3.2: Fresnel Coeffecients R for different values of θ

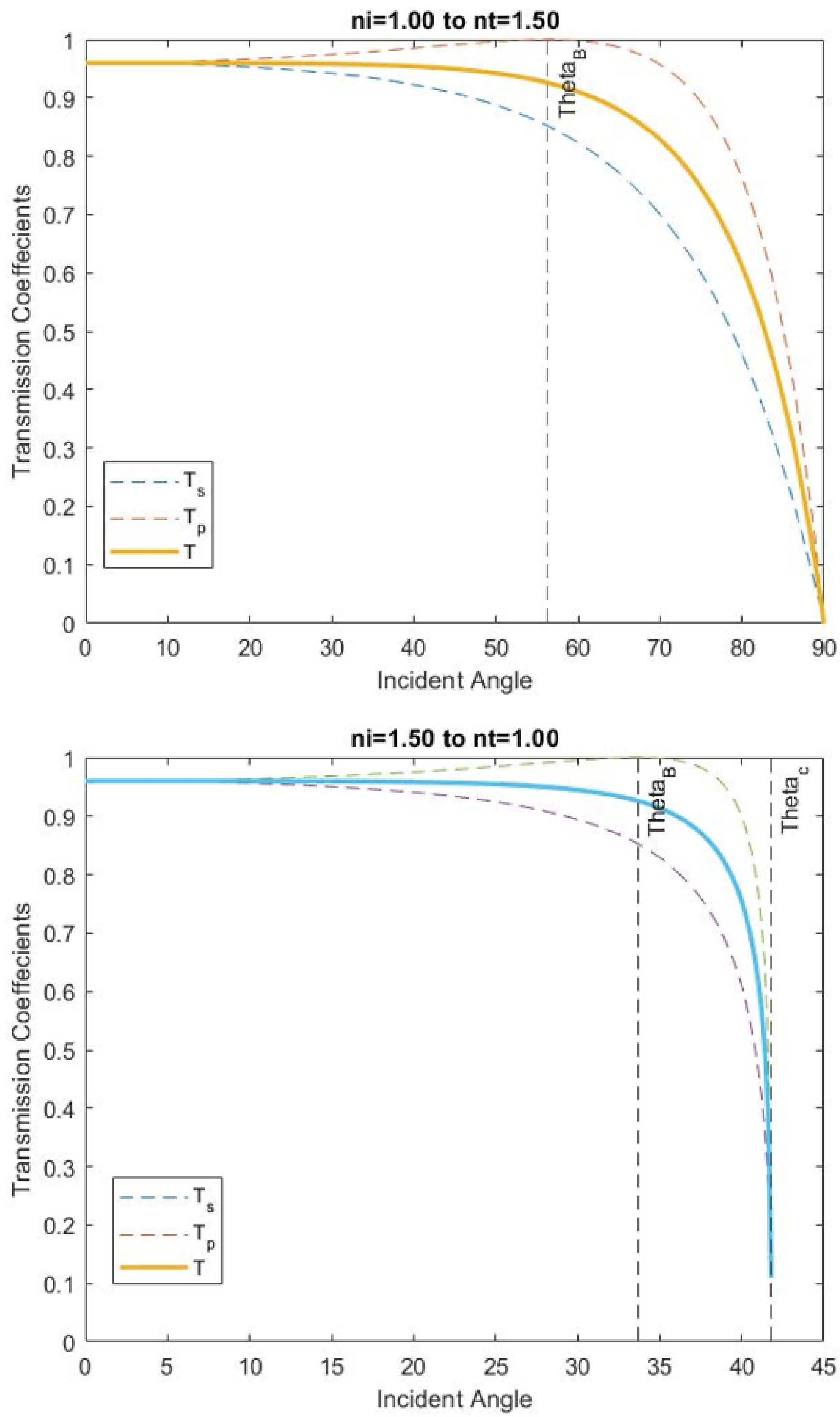

Figure 3.3: Fresnel Coeffecients T for different values of θ

the interface as the rays change direction [31]. The equations are:

$$\hat{\mathbf{s}}_q = \frac{\hat{\mathbf{k}}_{q-1} \times \hat{\boldsymbol{\eta}}_q}{\left|\hat{\mathbf{k}}_{q-1} \times \hat{\boldsymbol{\eta}}_q\right|}, \hat{\mathbf{p}}_q = \hat{\mathbf{k}}_{q-1} \times \hat{\mathbf{s}}_q, \hat{\mathbf{s}}'_q = \hat{\mathbf{s}}_q, \hat{\mathbf{p}}'_q = \hat{\mathbf{k}}_q \times \hat{\mathbf{s}}_q, \tag{3.7a}$$

$$\hat{\mathbf{s}}_q = \hat{\mathbf{s}}'_q = \hat{\mathbf{s}}'_{q-1}, \hat{\mathbf{p}}_q = \hat{\mathbf{k}}_{q-1} \times \hat{\mathbf{s}}_q, \hat{\mathbf{p}}'_q = \hat{\mathbf{k}}_q \times \hat{\mathbf{s}}_q \tag{3.7b}$$

$$\mathbf{O}_{in,q}^{-1} = \begin{pmatrix} \hat{s}_{x,q} & \hat{s}_{y,q} & \hat{s}_{z,q} \\ \hat{p}_{x,q} & \hat{p}_{y,q} & \hat{p}_{z,q} \\ \hat{k}_{x,q-1} & \hat{k}_{y,q-1} & \hat{k}_{z,q-1} \end{pmatrix}, \mathbf{O}_{\text{out },q} = \begin{pmatrix} \hat{s}_{x,q} & \hat{p}'_{x,q} & \hat{k}_{x,q} \\ \hat{s}_{y,q} & \hat{p}'_{y,q} & \hat{k}_{y,q} \\ \hat{s}_{z,q} & \hat{p}'_{z,q} & \hat{k}_{z,q} \end{pmatrix} \tag{3.7c}$$

$$\mathbf{E}_{sp,q-1} = \begin{pmatrix} E_{s,q-1} \\ E_{p,q-1} \\ 0 \end{pmatrix} = \mathbf{O}_{in,q}^{-1} \begin{pmatrix} E_{x,q-1} \\ E_{y,q-1} \\ E_{z,q-1} \end{pmatrix} \tag{3.7d}$$

$$\mathbf{E}_q = \mathbf{O}_{\text{out },q} \cdot \begin{pmatrix} E_{s,q} \\ E_{p',q} \\ 0 \end{pmatrix} = \begin{pmatrix} \hat{s}_{x,q}\hat{p}'_{x,q}\hat{k}_{x,q} \\ \hat{s}_{y,q}\hat{p}'_{y,q}\hat{k}_{y,q} \\ \hat{s}_{z,q}\hat{p}'_{z,q}\hat{k}_{z,q} \end{pmatrix} \cdot \begin{pmatrix} E_{s,q} \\ E_{p',q} \\ 0 \end{pmatrix} \tag{3.7e}$$

$$\mathbf{E}_q = E_{s,q} \begin{pmatrix} \hat{s}_{x,q} \\ \hat{s}_{y,q} \\ \hat{s}_{z,q} \end{pmatrix} + E_{p',q} \begin{pmatrix} \hat{p}'_{x,q} \\ \hat{p}'_{y,q} \\ \hat{p}'_{z,q} \end{pmatrix} \tag{3.7f}$$

$$\mathbf{E}_q = E_{s,q}\hat{\mathbf{s}}_q + E_{p',q}\hat{\mathbf{p}}'_q \tag{3.7g}$$

$$\mathbf{P}_q = \mathbf{O}_{\text{out },q}\mathbf{J}_{t,q}\mathbf{O}_{in,q}^{-1} \text{ and } \mathbf{P}_q = \mathbf{O}_{\text{out },q}\mathbf{J}_{r,q}\mathbf{O}_{in,q}^{-1}. \tag{3.7h}$$

This will provide us with polarization ray tracing matrix for reflection and refraction.

After calculating the power and polarization of the ray. The next step is the calculation of Force and Torque acting on the surface. which can be calculated through the relation

$$\mathbf{F}_{\text{Beam}} = \sum_m \mathbf{F}_{\text{ray}}^{(m)} = \sum_m \left[\frac{n_{\text{i}} P_{\text{i}}^{(m)}}{c} \hat{\mathbf{r}}_{\text{i}}^{(m)} - \frac{n_{\text{i}} P_{\text{r}}^{(m)}}{c} \hat{\mathbf{r}}_{\text{r},0}^{(m)} - \sum_{n=1}^{+\infty} \frac{n_{\text{i}} P_{\text{t},n}^{(m)}}{c} \hat{\mathbf{r}}_{\text{t},n}^{(m)} \right] \tag{3.8}$$

$$\begin{aligned} \mathbf{T}_{\text{ray}}^{(m)} = (\mathbf{P}_0 - \mathbf{C}) \times \frac{n_{\text{i}} P_{\text{i}}^{(m)}}{c} \hat{\mathbf{r}}_{\text{i}}^{(m)} - (\mathbf{P}_0 - \mathbf{C}) \times \frac{n_{\text{i}} P_{\text{r}}^{(m)}}{c} \hat{\mathbf{r}}_{\text{r},0}^{(m)} \\ - \sum_{n=1}^{+\infty} (\mathbf{P}_n - \mathbf{C}) \times \frac{n_{\text{i}} P_{\text{t},n}^{(m)}}{c} \hat{\mathbf{r}}_{\text{t},n}^{(m)}, \end{aligned} \tag{3.9}$$

where

$$\mathbf{T}_{\text{Beam}} = \sum_{m} \mathbf{T}_{\text{ray}}^{(m)}$$

The 'm' is for the number of rays and 'n' is the number of scattering events. In general, the power of the beam retained after 10 scattering events is minimal. For the case of a beam, ray's passes through a lens of numerical aperture, which focuses the beam to an object at study and the scattering events take place. The scattering event is shown in figure 3.4 for understanding.

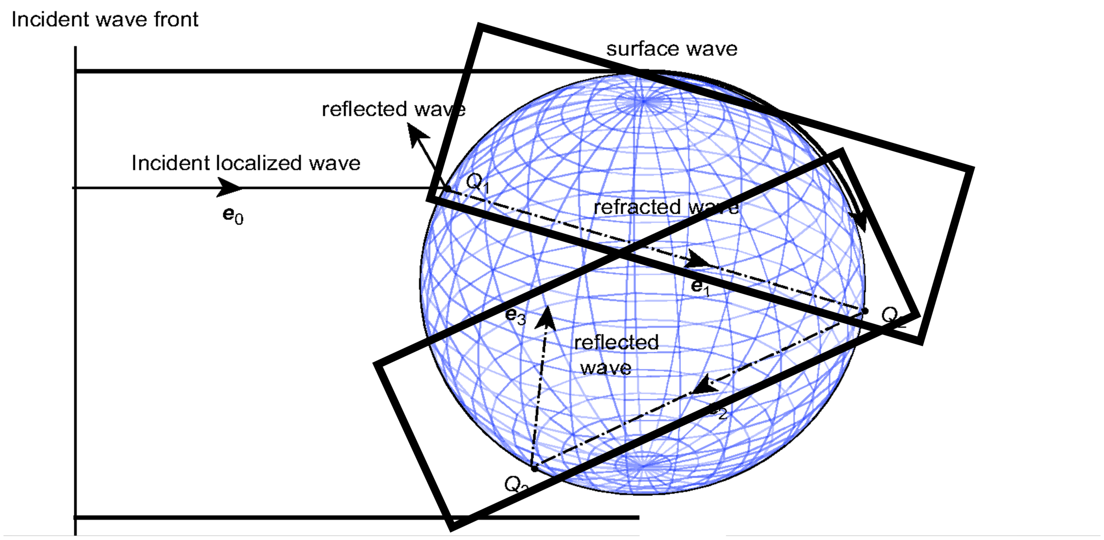

Figure 3.4: Scattering Events for a Sphere.

3.4 Code Validation

The validation of the BIL-OP was carried out with the data provided by Agnese Callegari group [28]. The results were in good agreement and are shown in fig (3.5) for circularly polarized light and in fig(3.6) for linearly polarized light.

The particle will be trapped as per the results in this section, which is also the case as seen through the experiments carried out in literature [32]. whenever a particle moves away from the centre of the beam (imagine beam applied at origin), a trapping force will act on the particle which will push the particle towards the centre of the beam, the force exerted by beam is small in pico-newtons (pN) but it has the potential to manipulate and trap particle in micro scale as can be seen in fig. 3.5 and 3.6. This idea validates the trapping potential of the beam. Due to this property of optical tweezers, they can be used for biology for manipulating the colloidal particle and tissue without damaging them.

3.5 Summary

An optical force and torque calculator is developed and validated for an optical potential utilizing the geometric ray approximation. The BIL-OP (in-house code) has the capability to effectively calculate the force and torque on an spherical particle. The results predict the behavior of trapping of dielectric particles which paves way for self-assembly, which has open studies for scientists to tackle challenges of great technological and economic impact such as the design and fabrication of biomimetic materials, bioremediation, and chemical sensing. The understanding of this behavior is critical in dealing with the challenges.

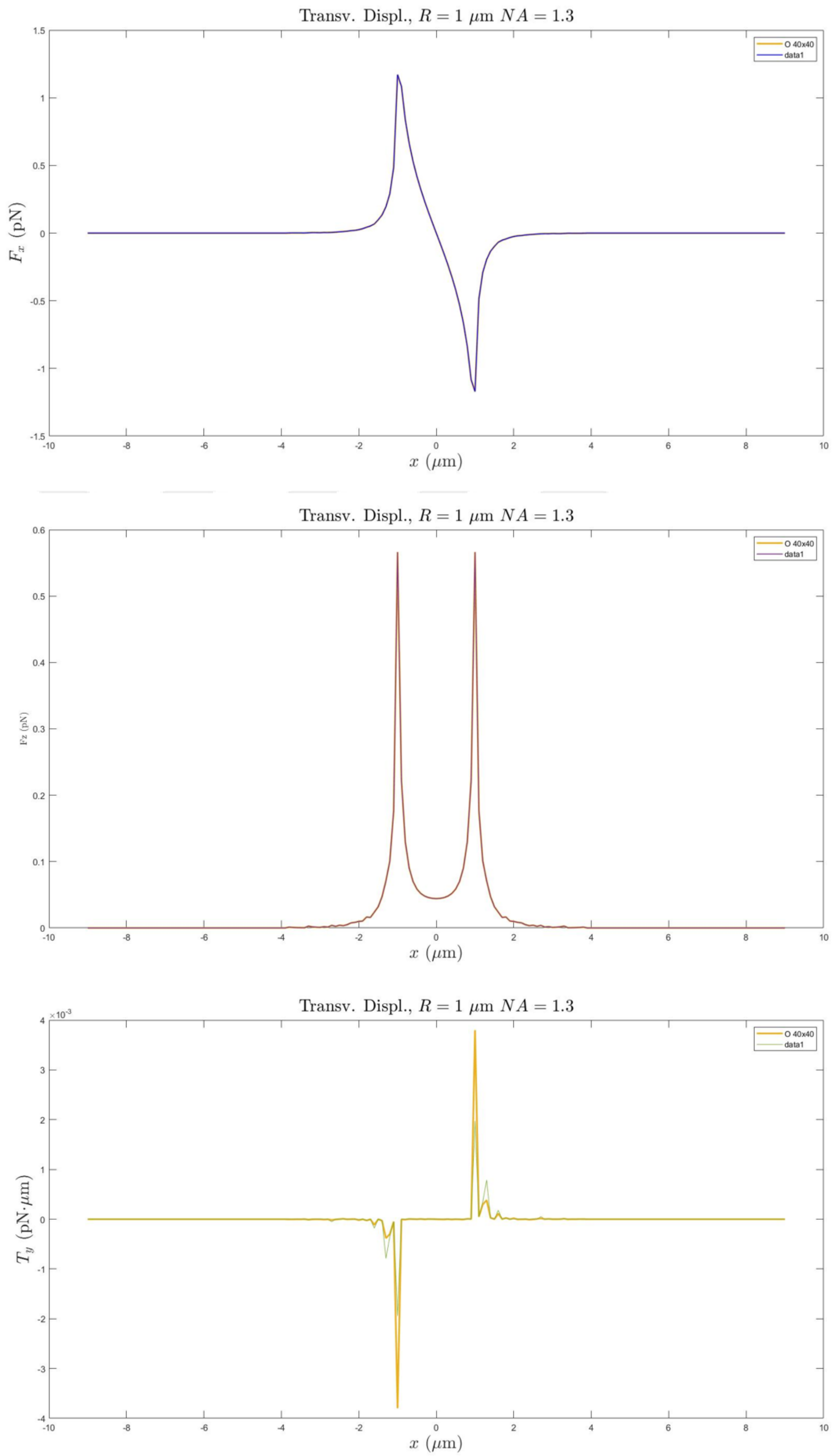

Figure 3.5: Forces and Torque (F_x F_z and T_y) comparison with Circularly polarized light.

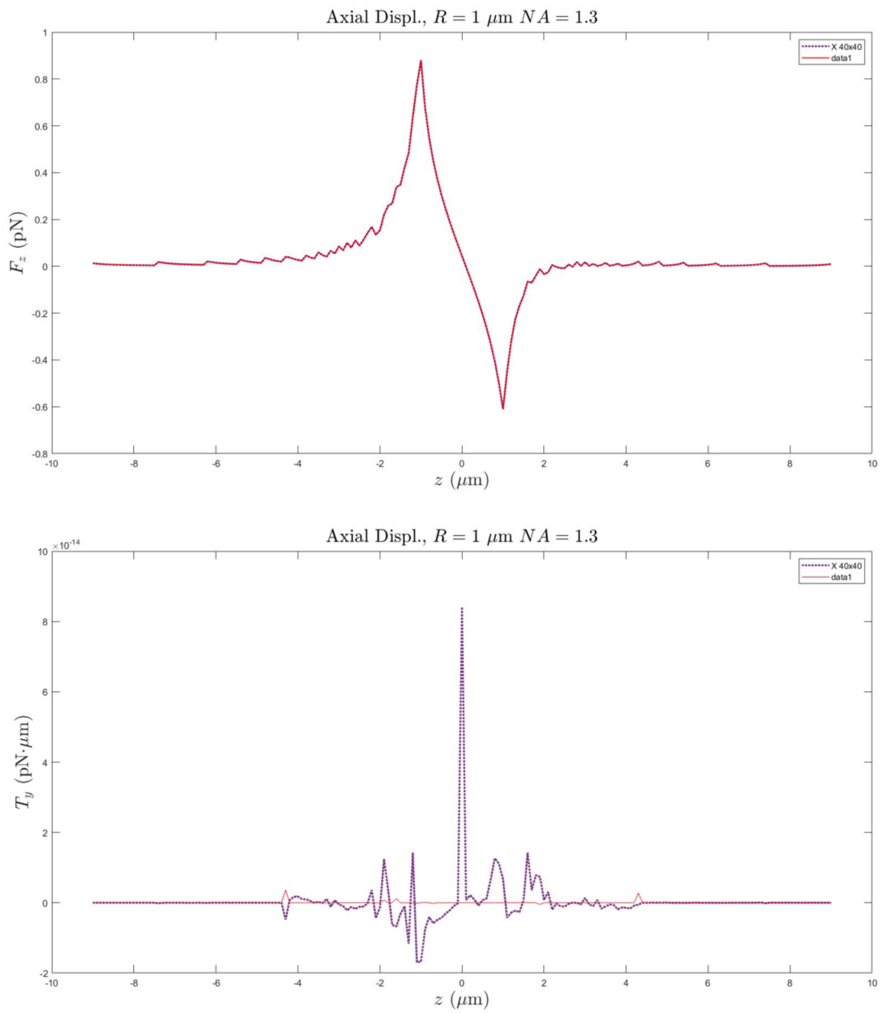

Figure 3.6: Force and Torque (F_z and T_y) comparison with linearly polarized light.

Chapter 4

Modelling Laser-Induced Heating in Optical Traps

4.1 Introduction

An effort was made to simulate the optical potential inside the system using the geometric ray approximation in the context of optical and fluid dynamic simulations. This paradigm calculated the thermal impacts on the fluid medium without taking into account the existence of individual particles. Instead, attention was focused on the fluid heating phenomena, and the complex interplay of energy transfer pathways was described using the governing energy equation.

The deliberate use of a mesh concentration method, in which the discretized representation of the computational domain was purposefully densified around crucial centers of interest, was a distinguishing aspect of this simulation. Using a 3-dimensional cylindrical coordinate system as the background for this tactical mesh refinement was a wise decision that complements the cylindrical symmetry frequently found in issues of this kind. By properly fitting the intricate geometry of the system, the adoption of this coordinate system aptly permitted the incorporation of spatial features.

The simulation's ability to determine the relative relevance of various forces operating within the system is one of its most noteworthy features. In particular, the contributions of the thermal force—which results from temperature differences and heat exchange processes—and the optical force—which results from the interaction between light and matter—were assessed. Careful examination revealed that the optical force far outweighed the effects of the heat force. In order to treat the thermal force as zero (negligible) within the parameters of the model, a re-confirmation using the geometric approximation was introduced.

In Section 4.2, The problem at hand was elaborated. In Section 4.3, The optical potential like Gaussian Beam, Hermite-Gaussian (HG)Beam and Cylindrical Vector Beam (CVB) are numerically obtained, In Section 4.4 the governing equations and numerical technique is briefly discussed . At last, the results are obtained through numerical simulations in Section 4.5, while a summary is provided in Section 4.6

4.1.1 Notations

The notation HG denotes the Hermite Gaussian Beam and CVB denotes the cylindrical Vector Beam, The $\boldsymbol{E}$ denotes the electric field. The symbol '$\boldsymbol{Q}$' denotes the source term in the energy equation. α denotes absorption coefficient and '$\boldsymbol{k}$' denotes the thermal conductivity of the fluid. '$\boldsymbol{I}$' is the intensity of the beam. ω is the beam waist.

4.2 Problem Statement

To model different optical potential (Optical Beam i.e. Gaussian beam, HG beam , CVB beams) and couple it with energy equation, it will act as the source. Similar to 3.3 the modelling of beam would be carried out by defining beams as rays as per the Geometric ray approximation. The beam would be assumed to be passing through a iris and an objective lens which will focus the beam. The electric field will be utilized to calculate the intensity and the Intensity will be related with heating and coupled with the fluid's energy equation to see the thermal effects in absence of particle.

4.3 Optical Potential

The Beams are defined by their electric field distribution (E). we will use the geomtric ray approximation to model the optical potentials.

Gaussian Beam 4.3.1.
The Gaussian Beam is defined as:

$$\mathbf{E}^{\mathrm{G}}(\rho, z) = \mathbf{E}_0 \frac{w_0}{w(z)} e^{-\frac{\rho^2}{u(z)^2}} e^{+ik_{\mathrm{m}}z - i\zeta(z) + ik_{\mathrm{m}}\frac{\rho^2}{2R(z)}}, \tag{4.1}$$

where;

$$w(z) = w_0 \sqrt{1 + \frac{z^2}{z_0^2}}, \quad \approx \omega(z) = \omega_0 \sqrt{1 + \left(\frac{z\lambda_0}{\pi n_m \omega_0^2}\right)^2}, \tag{4.2}$$

$$R(z) = z\left(1 + \frac{z_0^2}{z^2}\right) \tag{4.3}$$

$$\zeta(z) = \operatorname{atan}\left(\frac{z}{z_0}\right) \tag{4.4}$$

$$k_{\mathrm{m}} = |\mathbf{k}_{\mathrm{m}}| = \frac{n_{\mathrm{m}}\omega}{c} = \frac{2\pi}{\lambda_{\mathrm{m}}} \tag{4.5}$$

$$I = \frac{1}{2}\frac{c}{n_{\mathrm{m}}}\varepsilon_{\mathrm{m}}|E|^2. \tag{4.6}$$

we applied the paraxial approximation at each slice in Z and obtained the electric field. The Gaussian beam obtained numerically is:

Hermite-Gaussian Beam 4.3.2.
The Hermite-Gaussian Beam is defined as:

$$\mathbf{E}^{\mathrm{HG}}_{m_x m_y}(x, y, z) = \mathbf{E}^{\mathrm{G}}(x, y, z) H_{m_x}\left(\sqrt{2}\frac{x}{w(z)}\right) H_{m_y}\left(\sqrt{2}\frac{y}{w(z)}\right) e^{-i(m_x+m_y)\zeta(z)} \tag{4.7}$$

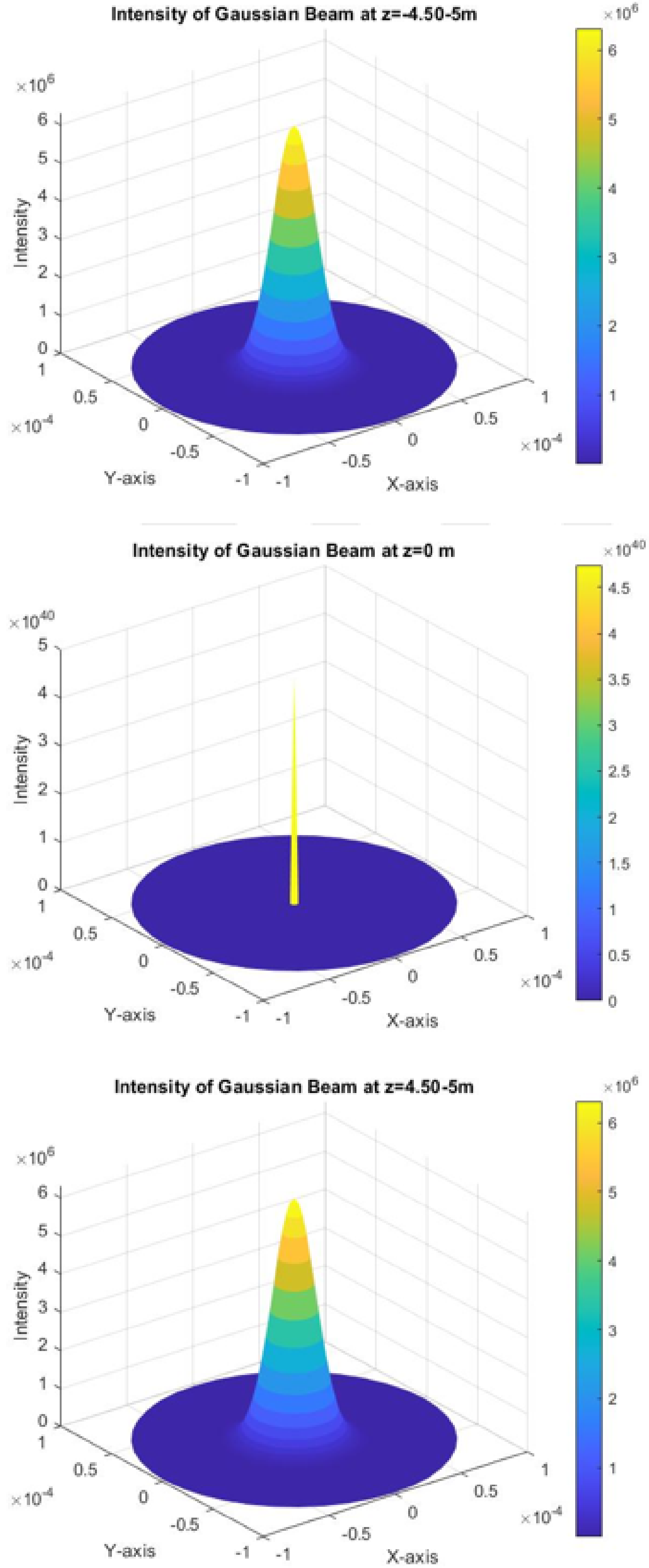

Figure 4.1: Intensity Distribution of Gaussian Beam at different Z locations.

where variables are same as eq. 4.2 4.3,4.4,4.5 and 4.6.

we applied the paraxial approximation at each slice in Z and obtained the electric field. The Hermite-Gaussian beam obtained numerically is shown in fig. 4.2:

Cylindrical Vector Beam 4.3.3.
The Cylindrical Vector Beam is defined as:

$$\mathbf{E}_r^{\mathrm{CVB}}(x,y,z) = E_{10}^{\mathrm{HG}}(x,y,z)\hat{\mathbf{x}} + E_{01}^{\mathrm{HG}}(x,y,z)\hat{\mathbf{y}} \tag{4.8}$$

where variables are same as eq. 4.2 4.3,4.4,4.5 and 4.6 and '0' and '1' defines the modes of the Hermite-Gaussian Beam.

we applied the paraxial approximation at each slice in Z and obtained the electric field. The CVB beam obtained numerically (electric field and Intensities) is shown in fig. 4.3 and 4.4:

4.4 Modelling Fluid-Optics Coupling

The modelling of fluid heated due to the optical potential applied is carried out, the flow is assumed to be stationary and in steady state. as per the assumption the energy equation is:

$$\nabla \cdot (k\nabla T) + Q = 0 \tag{4.9}$$

The 'Q' is the source term in the energy equation. The source term will be the variable which will couple the energy equation and optical potential. The Electric field calculated will result in calculation of intensity distribution ('I') of the beam. The source term and intensity relationship is as follows:

$$Q = 2\alpha I \tag{4.10}$$

The problem at hand will be solved by employing the Cylindrical co-ordinates system (ρ,θ,z). The non-uniform mesh was employed as close to the centre (focus

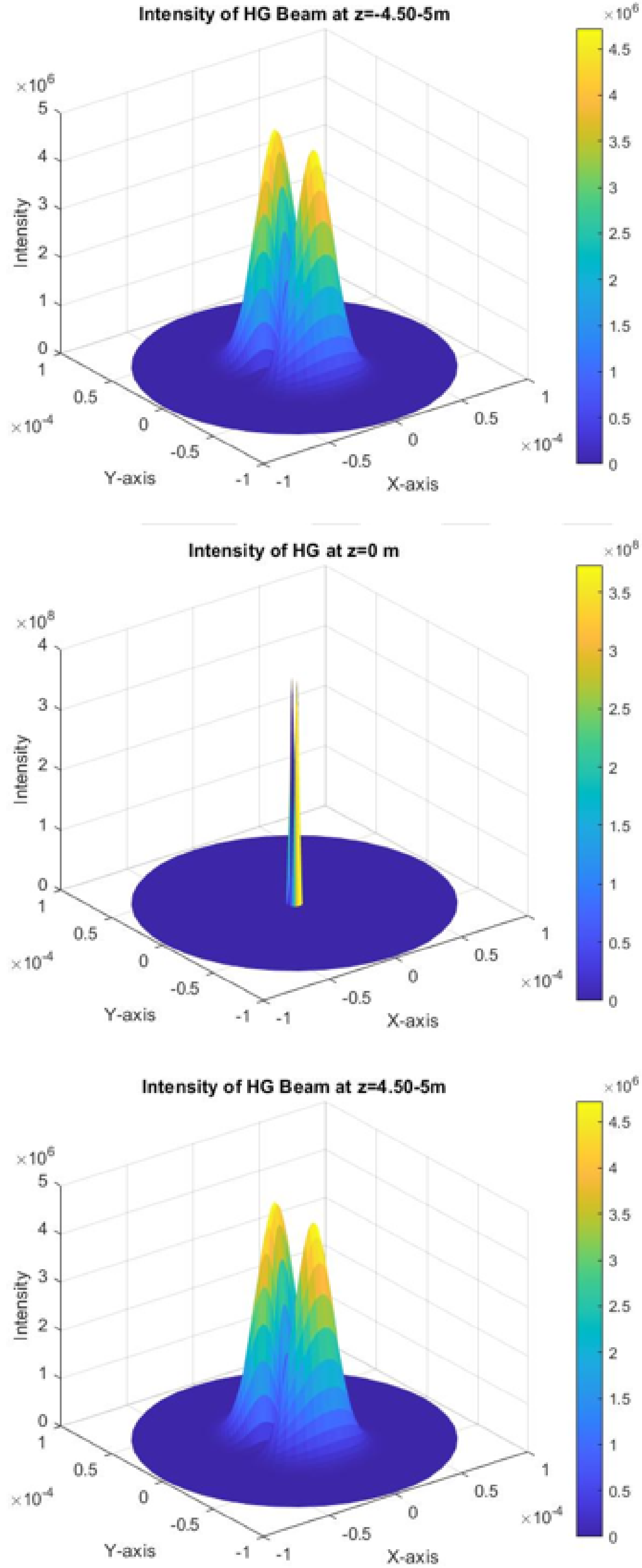

Figure 4.2: Intensity Distribution of Hermite-Gaussian Beam at different Z locations.

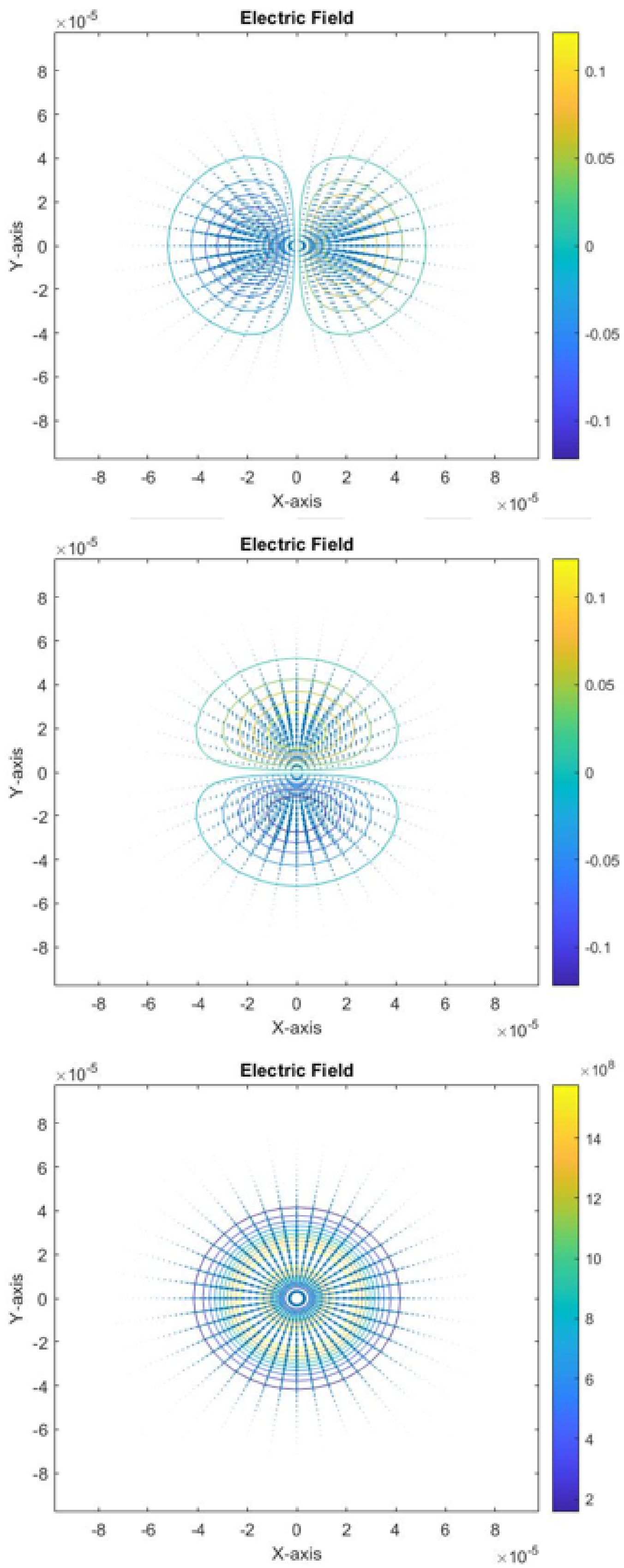

Figure 4.3: Electric Field Distribution of CVB_r at different Z locations.

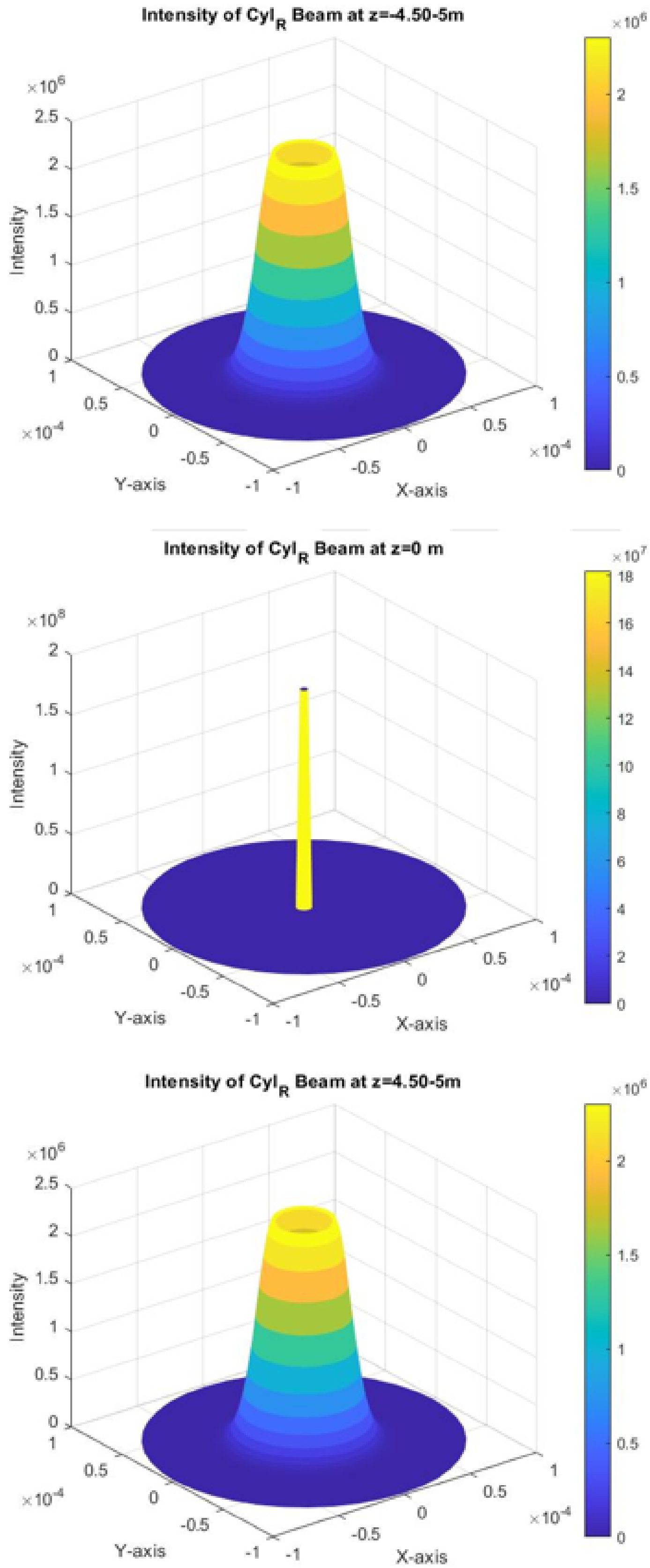

Figure 4.4: Intensity Distribution of CVB$_r$ at different Z locations.

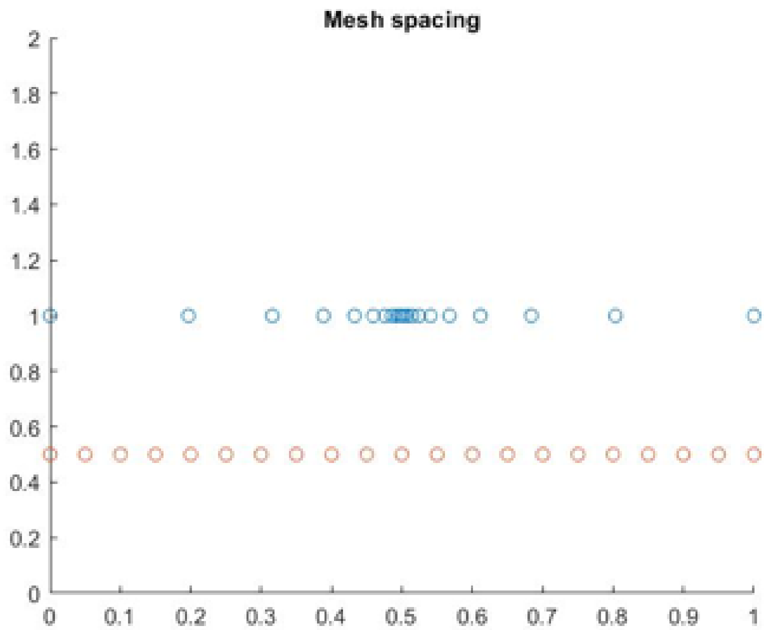

Figure 4.5: Mesh points in 1D.

point) more point descritization was required to achieve better results. The mesh is as show in fig 4.5:

The numerical technique used to solve the problem is shown in eq. 4.11 and 4.12.

$$f_i' = \frac{f_{i+1} - \left(\frac{h_i}{h_{i-1}}\right)^2 f_{i-1} - \left[1 - \left(\frac{h_i}{h_{i-1}}\right)^2\right] f_i}{h_i \left(1 + \frac{h_i}{h_{i-1}}\right)} \tag{4.11}$$

$$f_i'' = \frac{2\left[f_{i+1} + \frac{h_i}{h_{i-1}} f_{i-1} - \left(1 + \frac{h_i}{h_{i-1}}\right) f_i\right]}{h_i h_{i-1} \left(1 + \frac{h_i}{h_{i-1}}\right)} \tag{4.12}$$

The Velocities will be calculated through the relation

$$\bar{V} = -D_t \nabla T \tag{4.13}$$

where D_t is the diffusion Constant. and the force will be calculated through the relation, which is derived from the stokes drag force.

$$F = 6\pi\eta r V \tag{4.14}$$

4.5 Numerical Simulations

The numerical simulation were carried out until the difference between the consecutive iterations were $\leq 1e^{-3}$. The parameters are shown in Table 4.1.

Table 4.1: Numerical Values.

P	7mW
k	0.599
w_0	0.4μm
f	100μm
NA	1.3
Depth	180μm
λ	976 nm
α	50

The Temperature Profile are shown in fig: 4.6.as we can see the temperature raised by beam of fluid (which is water in our case) is quite small even if the beam is highly focused.
The temperature profile is used to calculate the forces utilizing the equation 4.14. The force distribution for each of the beam is depicted in fig 4.7 4.8 and 4.9. The Force comparison reveals that the forces exerted by the beam heating the fluid is almost 1000 time less than the forces exerted by the light beam on the particle (optical force).

4.6 Summary

This chapter provides the force estimation by calculating the temperature distribution in the fluid in absence of the particle. The force caused by heating of the fluid is in femto-newtons. The heat equation was numerically solved with with the beam coupled through the source term. The results dictates that it is reasonable to ignore the force caused by fluid which is heated with a laser beam of low power (in mW's). Hence, The effect of fluid being heated can be ignored and utilization of this approximation is reasonable.

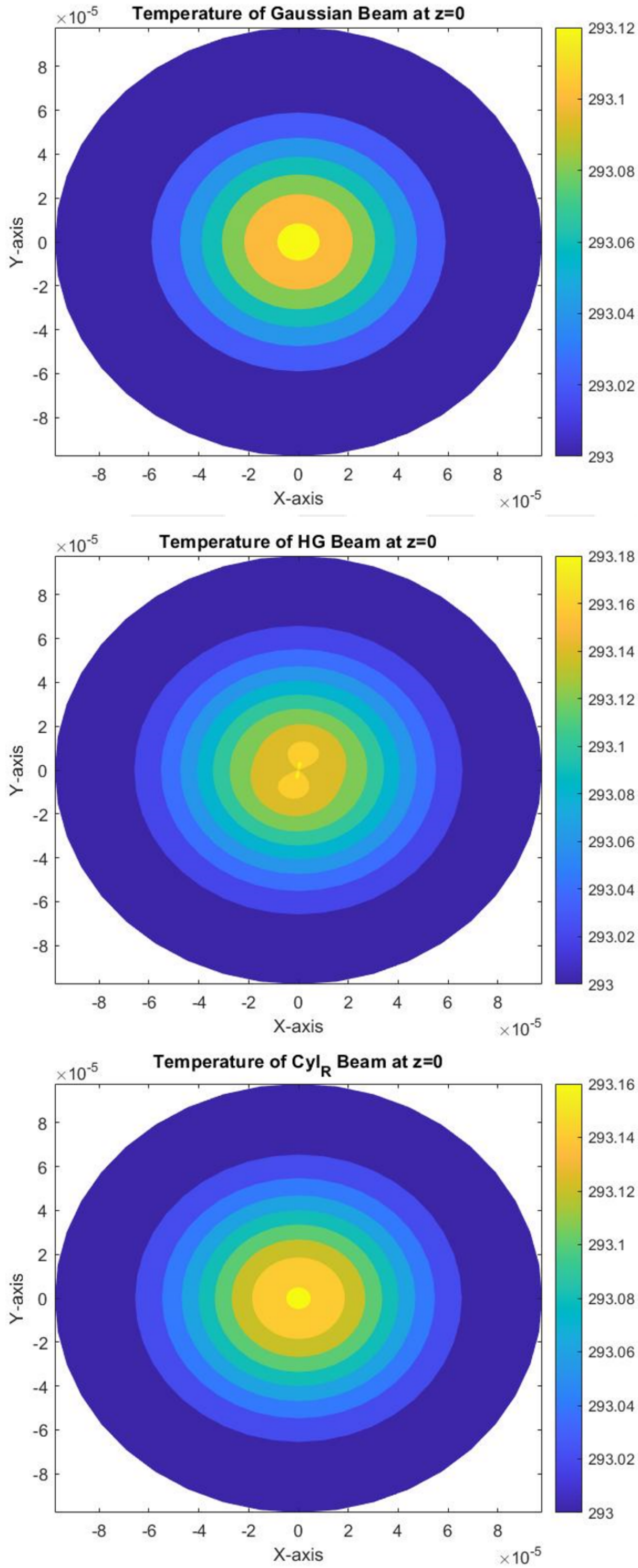

Figure 4.6: Temperature Distribution of different beams.

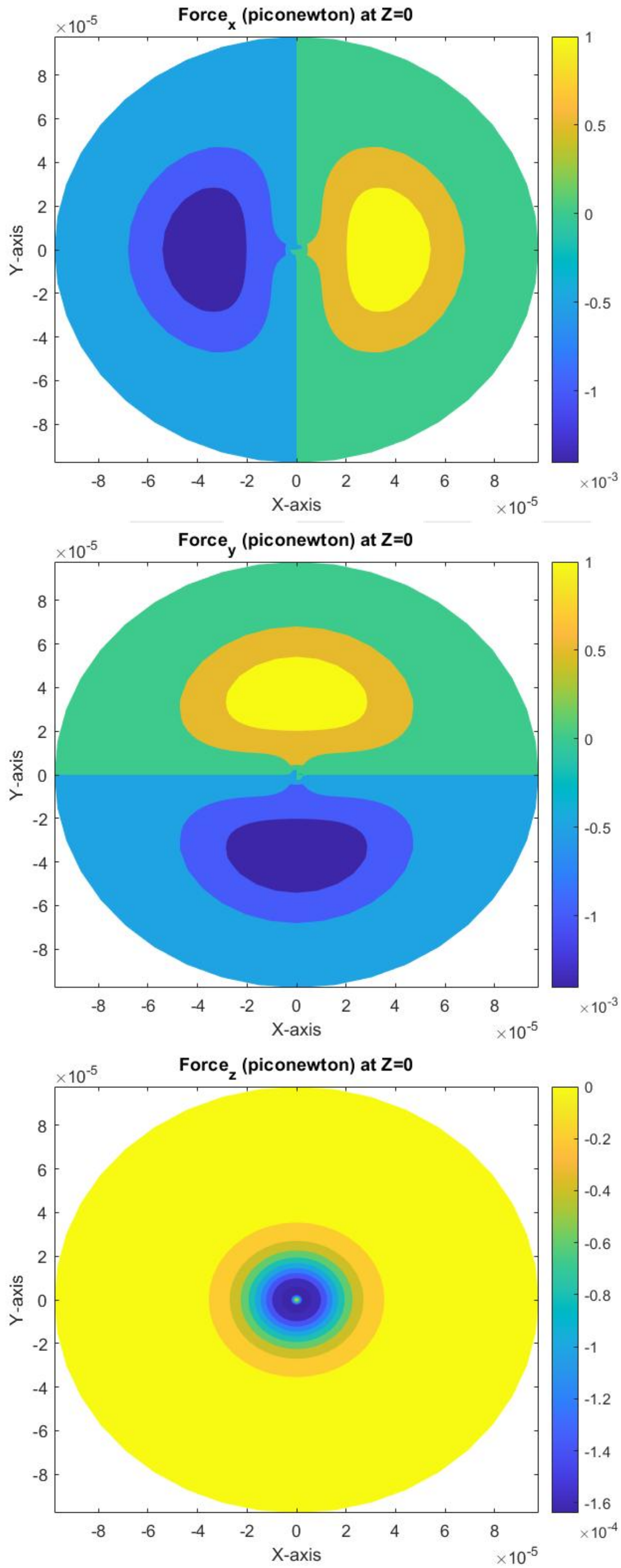

Figure 4.7: Force Distribution of Gaussian beam.

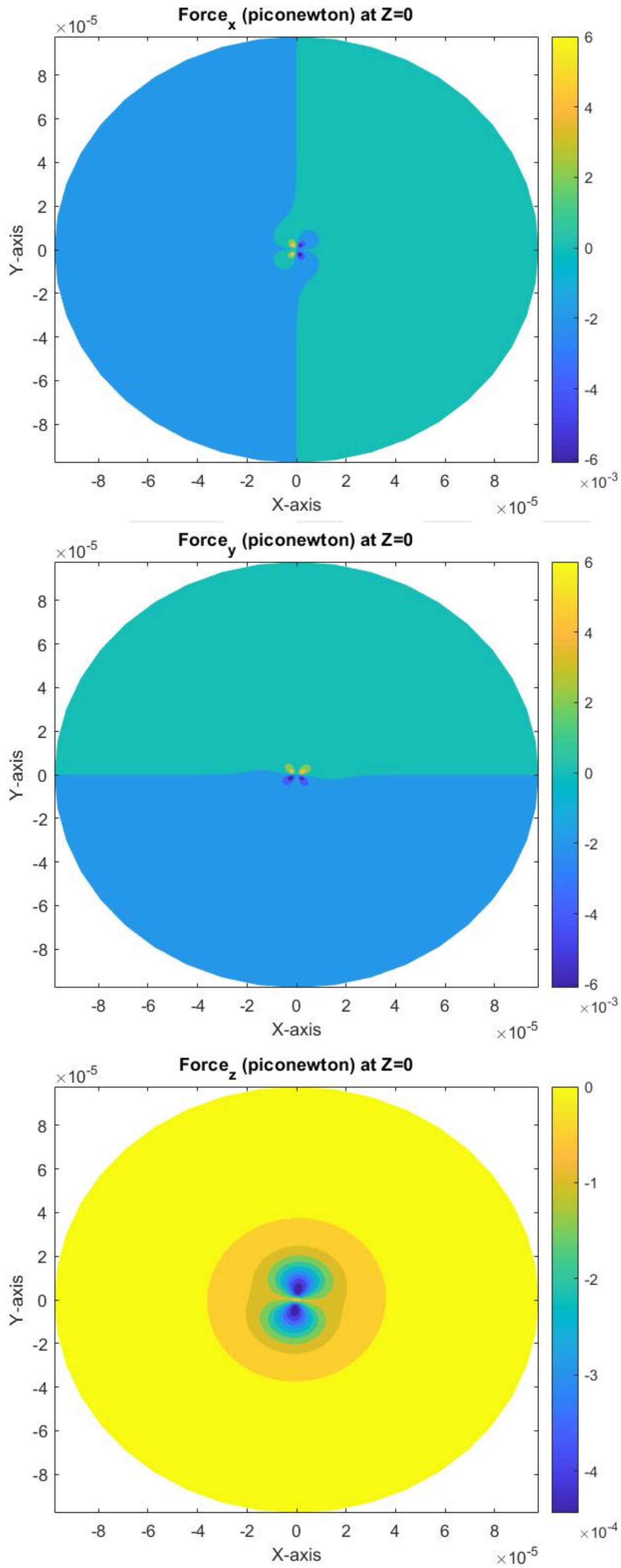

Figure 4.8: Force Distribution of Hermite Gaussian beam.

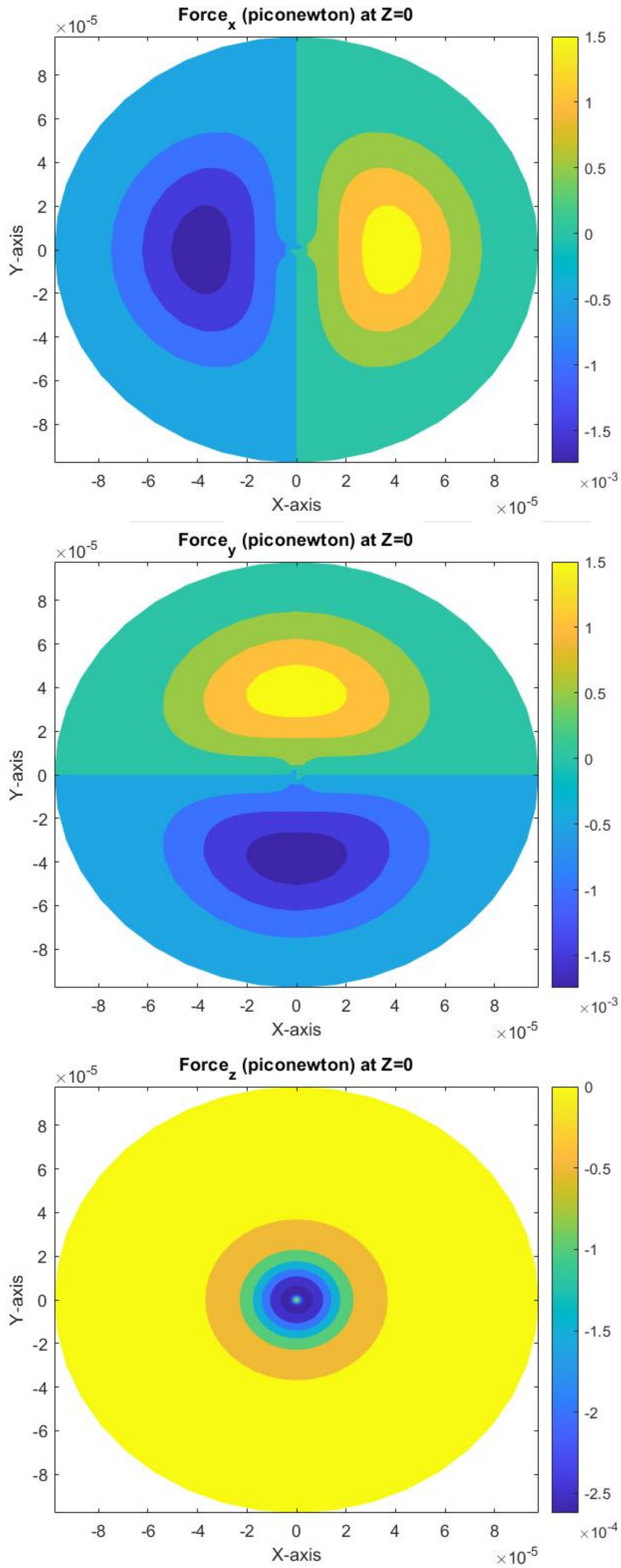

Figure 4.9: Force Distribution of Cylindrical Vector beam.

Chapter 5

Conclusion

In this thesis, A multidisciplinary problem was solved while focusing on the three major aspects 1) Thermal Distribution 2) Optical effects and 3) Laser-induced heating. The three aspects of the problems were individually considered. The aim of the optical part was to develop an optical package which can effectively calculate the forces and torques acting on a particle. The results indicated the ability of the optical traps to trap and manipulative the particles towards the centre of the beam. in respect of the thermal effects, we considered the thermal effects in two ways, in one case we only considered the effect of the optical potential induced fluid heating in the absence of the particle at study and other in which the absorbing part of the Janus particle act as a source term and effect the fluid behavior around it. For the fluid heating, the results provides strong ground for the argument that the laser-induced affects due optical potential are negligible and can be ignored as the force caused by the temperature gradient is 10^{-3} times less than optical force. The other important aspect from this study was understanding and numerical implementation of different optical beams (HG, CVB) which can be used with the optical package to study their behavior. For the case of Janus sphere acting as a source term. The results provide strong grounds for the argument that the thermal forces are not negligible and are important. The vorticity and drag force as indicated by results have a linear relationship with Grashoff number, Beam Intensity and Beam waist. The vorticity and drag force increase almost linearly with Grashoff number, Beam intensity and waist in cap-up and cap-down configuration only exception is the pressure drag whose behavior becomes opposite and decreases linearly in cap-up configuration.

Bibliography

[1] G. G. Stokes *et al.*, "On the effect of the internal friction of fluids on the motion of pendulums," *Transactions of the Cambridge Philosophical Society*, vol. IX, p. 8, 1851.

[2] C. Williamson, "Evolution of a single wake behind a pair of bluff bodies," *Journal of Fluid Mechanics*, vol. 159, pp. 1–18, 1985.

[3] S. Taneda, "Experimental investigation of the wake behind a sphere at low reynolds numbers," *Journal of the physical society of Japan*, vol. 11, no. 10, pp. 1104–1108, 1956.

[4] A. Whitehead, "Second approximations to viscous fluid motion," *Quart. J. Math*, vol. 23, no. 1, pp. 143–152, 1889.

[5] I. Proudman and J. Pearson, "Expansions at small reynolds numbers for the flow past a sphere and a circular cylinder," *Journal of Fluid Mechanics*, vol. 2, no. 3, pp. 237–262, 1957.

[6] C. Oseen, "Stokes' formula and a related theorem in hydrodynamics," *Arkiv. Mat. Astron. Fysik*, vol. 6, no. 20, 1910.

[7] S. Kaplun and P. Lagerstrom, "Asymptotic expansions of navier-stokes solutions for small reynolds numbers," *Journal of Mathematics and Mechanics*, pp. 585–593, 1957.

[8] M. Van-Daik, "Perturbation methods in fluid mechanics," *M., Mir,–1967*, 1964.

[9] M. Kohr *et al.*, "An application of the method of matched asymptotic expansions for low reynolds number flow past a cylinder of arbitrary cross section," *International Journal of Mathematics and Mathematical Sciences*, vol. 2004, pp. 2525–2535, 2004.

[10] A. Umemura, "Matched-asymptotic analysis of low-reynolds-number flow past two equal circular cylinders," *Journal of Fluid Mechanics*, vol. 121, pp. 345–363, 1982.

[11] S. Datta and S. Singhal, "Small reynolds number steady flow past a sphere with a source at its centre," *Applications and Applied Mathematics: An International Journal (AAM)*, vol. 6, no. 1, p. 16, 2011.

[12] A. J. Chorin, "The numerical solution of the navier-stokes equations for an incompressible fluid," *Bulletin of the American Mathematical Society*, vol. 73, no. 6, pp. 928–931, 1967.

[13] C. Christov and P. Volkov, "Numerical investigation of the steady viscous flow past a stationary deformable bubble," *Journal of Fluid Mechanics*, vol. 158, pp. 341–364, 1985.

[14] B. Fornberg, "Steady viscous flow past a sphere at high reynolds numbers," *Journal of Fluid Mechanics*, vol. 190, pp. 471–489, 1988.

[15] L. B. Zhang, "A second-order upwinding finite difference scheme for the steady navier-stokes equations in primitive variables in a driven cavity with a multigrid solver," *ESAIM: Mathematical Modelling and Numerical Analysis*, vol. 24, no. 1, pp. 133–150, 1990.

[16] G. Juncu, "A numerical study of steady viscous flow past a fluid sphere," *International journal of heat and fluid flow*, vol. 20, no. 4, pp. 414–421, 1999.

[17] M.-C. Lai, "Fourth-order finite difference scheme for the incompressible navier–stokes equations in a disk," *International journal for numerical methods in fluids*, vol. 42, no. 8, pp. 909–922, 2003.

[18] Z. Li and C. Wang, "A fast finite differenc method for solving navier-stokes equations on irregular domains," *Communication Math Science*, vol. 1, no. 1, pp. 180–196, 2003.

[19] A. Hamielec, T. Hoffman, and L. Ross, "Numerical solution of the navier-stokes equation for flow past spheres: Part i. viscous flow around spheres with and without radial mass efflux," *AIChE Journal*, vol. 13, no. 2, pp. 212–219, 1967.

[20] T. Bickel, A. Majee, and A. Würger, "Flow pattern in the vicinity of self-propelling hot janus particles," *Physical Review E*, vol. 88, no. 1, p. 012301, 2013.

[21] V. Jenson, "Viscous flow round a sphere at low reynolds numbers (¡ 40)," *Proceedings of the Royal Society of London. Series A. Mathematical and Physical Sciences*, vol. 249, no. 1258, pp. 346–366, 1959.

[22] A. Ashkin, "Optical trapping and manipulation of neutral particles using lasers," *Proceedings of the National Academy of Sciences*, vol. 94, no. 10, pp. 4853–4860, 1997.

[23] K. C. Neuman and A. Nagy, "Single-molecule force spectroscopy: optical tweezers, magnetic tweezers and atomic force microscopy," *Nature methods*, vol. 5, no. 6, pp. 491–505, 2008.

[24] K. Dholakia and T. Čižmár, "Shaping the future of manipulation," *Nature photonics*, vol. 5, no. 6, pp. 335–342, 2011.

[25] M. Padgett and R. Bowman, "Tweezers with a twist," *Nature photonics*, vol. 5, no. 6, pp. 343–348, 2011.

[26] M. L. Juan, M. Righini, and R. Quidant, "Plasmon nano-optical tweezers," *Nature photonics*, vol. 5, no. 6, pp. 349–356, 2011.

[27] O. M. Marago, P. H. Jones, P. G. Gucciardi, G. Volpe, and A. C. Ferrari, "Optical trapping and manipulation of nanostructures," *Nature nanotechnology*, vol. 8, no. 11, pp. 807–819, 2013.

[28] A. Callegari, M. Mijalkov, A. B. Gököz, and G. Volpe, "Computational toolbox for optical tweezers in geometrical optics," *JOSA B*, vol. 32, no. 5, pp. B11–B19, 2015.

[29] A. Ashkin, J. M. Dziedzic, J. E. Bjorkholm, and S. Chu, "Observation of a single-beam gradient force optical trap for dielectric particles," *Optics letters*, vol. 11, no. 5, pp. 288–290, 1986.

[30] P. Polimeno, A. Magazzu, M. A. Iati, F. Patti, R. Saija, C. D. E. Boschi, M. G. Donato, P. G. Gucciardi, P. H. Jones, G. Volpe, *et al.*, "Optical tweezers and their applications," *Journal of Quantitative Spectroscopy and Radiative Transfer*, vol. 218, pp. 131–150, 2018.

[31] R. Chipman, W. S. T. Lam, and G. Young, *Polarized light and optical systems*. CRC press, 2018.

[32] M. Tassieri, *Microrheology with Optical Tweezers: Principles and Applications*. CRC Press, 2016.